



HAL
open science

Measurement prototype for fast estimation of building wall thermal resistance under controlled and natural environmental conditions

Thanh-Tung Ha, Vincent Feuillet, Julien Waeytens, Kamel Zibouche, Laurent Peiffer, Yann Garcia, Véronique Le Sant, Rémi Bouchie, Alain Koenen, Jean-Pierre Monchau, et al.

► To cite this version:

Thanh-Tung Ha, Vincent Feuillet, Julien Waeytens, Kamel Zibouche, Laurent Peiffer, et al.. Measurement prototype for fast estimation of building wall thermal resistance under controlled and natural environmental conditions. *Energy and Buildings*, 2022, 268, pp.112166. 10.1016/j.enbuild.2022.112166 . hal-04119869

HAL Id: hal-04119869

<https://hal.u-pec.fr/hal-04119869v1>

Submitted on 22 Jul 2024

HAL is a multi-disciplinary open access archive for the deposit and dissemination of scientific research documents, whether they are published or not. The documents may come from teaching and research institutions in France or abroad, or from public or private research centers.

L'archive ouverte pluridisciplinaire **HAL**, est destinée au dépôt et à la diffusion de documents scientifiques de niveau recherche, publiés ou non, émanant des établissements d'enseignement et de recherche français ou étrangers, des laboratoires publics ou privés.



Distributed under a Creative Commons Attribution - NonCommercial 4.0 International License

Measurement prototype for fast estimation of building wall thermal resistance under controlled and natural environmental conditions

Thanh-Tung HA^a, Vincent FEUILLET^{*,a}, Julien WAEYTENS^b, Kamel ZIBOUCHE^c, Laurent PEIFFER^d, Yann GARCIA^e, Véronique LE SANT^e, Rémi BOUCHIE^c, Alain KOENEN^e, Jean-Pierre MONCHAU^f, Laurent IBOS^a

^aUniv Paris Est Creteil, CERTES, F-94010 Creteil, France

^bUniv Gustave Eiffel, IFSTTAR, Cité Descartes, 14-20 Boulevard Newton, 77420 Champs-sur-Marne, France

^cCentre Scientifique et Technique du Bâtiment (CSTB), 84 Avenue Jean Jaurès, 77420 Champs-sur-Marne, France

^dCerema, 71 Rue de la Grande Haie, 54510 Tomblaine, France

^eLaboratoire National de Métrologie et d'Essais (LNE), 29 Rue Roger Hennequin, 78197 Trappes, France

^fTHEMACS Ingénierie, 2bis rue Alfred Nobel, 77420 Champs-sur-Marne, France

Abstract

Most of the methods for *in situ* measurement of the thermal resistance of building walls implement passive approaches requiring long measurement times and specific environmental conditions. In the literature, different active approaches have been studied but they remain limited in terms of applications and do not systematically lead to short identification times. This article that follows a previous numerical benchmark study presents a new measurement prototype using a lamp box which heats up one of the surfaces (typically the interior surface) of the wall to be characterized. The use of an aluminum plate placed in contact with the wall face subjected to thermal excitation enables the homogenization of the heat flux transmitted to the wall. Three inverse procedures are implemented to estimate the thermal resistance of the studied wall. The originality of this work comes from an exhaustive measurement campaign. On the one hand, four types of wall among the most common in France, *i.e.* **Internal Insulation Wall, External Insulation Wall and Wood Frame Wall specially built for this study and a Single Concrete Wall located in a real building**, were investigated. On the other hand, the

use of different climatic chambers made it possible to generate many different environmental conditions (constant, variable and natural). The results highlight the possibilities offered by this *in situ* experimental device for estimating in a few hours (6 to 10 hours) the thermal resistance of the wall studied or of its first layers, as well as the limits depending on the type of wall and the environmental conditions. Some operational recommendations are also provided: avoiding thermal bridges, solar protection in case of strong sunlight on the exterior side of the wall and location of the device on the exterior side in the case of the **External Insulation Wall**.

Keywords: Building walls, Thermal resistance, *In situ* measurement, Active method, Inverse problem.

* Corresponding author. *E-mail address:* vincent.feuillet@u-pec.fr

1. Introduction

According to recent surveys, the building sector is currently the third largest contributor to primary energy consumption in the EU [1] (about 20% of total energy use) and is considered to be one of the main potential sources of energy savings, in particular by improving the thermal insulation of buildings. In France, about two-thirds of the buildings (apartment blocks, private houses, etc.) were built before the first thermal regulation in 1975 and are generally sources of important energy losses. Renovation works have been undertaken to improve resident thermal comfort and achieve an overall energy saving objective. In 2012, the French thermal regulation RT2012 [2] fixed a limit of primary energy consumption at $50 \text{ kWh}\cdot\text{m}^{-2}\cdot\text{year}^{-1}$ and entailed a requirement of thermal insulation for new or renovated buildings. The thermal insulation of a building envelope can be assessed by the thermal resistance value (or by the thermal transmittance value). The consumption objectives imposed by the RT2012 result in a minimum resistance value of about $4 \text{ m}^2\cdot\text{K}\cdot\text{W}^{-1}$ for an opaque building wall. In comparison, this value was $3 \text{ m}^2\cdot\text{K}\cdot\text{W}^{-1}$ according to the consumption objectives of the previous RT2005. It is also important to note that these requirements will continue to increase in the next regulation.

Global *in situ* methods exist for identifying the overall thermal performance of a building envelope. This was the subject of European projects [3] and Annex 58 of the IEA [4]. Two approaches are currently used to evaluate

the overall performance of the envelope: identification methods based on indirect measurements performed in occupied buildings [5, 6] and measurement methods under controlled heating conditions in unoccupied building [4, 7, 8]. However several points must be checked before knowing if a building satisfies the insulation requirement. In the case of a new building, the global heat transfer coefficient of the envelope must be estimated, but an old building involves detecting the parts of the building requiring renovation. All of these works need a robust *in situ* measurement method for determining the insulation level, or thermal resistance value, of a given wall in a building, and not only the global U -value of the building.

Research works have been conducted to develop an efficient method for estimating an opaque building wall thermal resistance and are based on two main approaches. The first type aims to implement a passive method which consists in monitoring a building wall while it reacts naturally with its environment. Experimental data are collected by using thermal sensors (for instance, thermocouple or infrared (IR) camera and heat flux meter) for further qualitative or quantitative studies. Many studies [9, 10, 11, 12] concerning the thermal resistance estimation in passive mode are derived from the following two standards: ISO 8990 [13] and ISO 9869-1 [14], with extension ISO 9869-2 [15]. Both methods use a heat flux meter and thermocouples or IR camera to measure the heat flux through the wall in quasi steady-state regime, which leads to long measurement times (generally between 24 to 72 hours). ISO 8990 standard is only available under laboratory conditions (climatic chambers) while ISO 9869-1 standard is dedicated to *in situ* measurement under specific environmental conditions (wall type and orientation, temperature gradient across the wall, weather conditions). Instead of using a heat flux meter, some approaches propose to compute the heat flux across the wall from the temperature captured by an IR camera or a thermocouple [16, 17, 18, 19, 20, 21]. These works involve the calculation of the heat transfer coefficient by convection, generally difficult to estimate *in situ*. For instance, values from ISO 6946 standard [22] were used in [20] and empirical correlations were used in [21]. There are also passive studies using a transient physical modeling associated to IR thermography or thermocouple measurements to assess wall thermal resistance. Petojevic et al. [23] used the thermal impulse response as model and Tikhonov regularization technique for estimating parameters while Larbi Youcef et al. [24] used Finite Elements and Levenberg-Marquardt optimization algorithm. Biddulph et al. carried out a Bayesian estimation method [25] for simultaneously esti-

inating thermal resistance and effective thermal mass, method subsequently improved by Gori et al. [26]. Another work [27] proposed the development of a Bayesian approach allowing the determination of the thermal properties of a wall (U -value and C -value) and their associated uncertainties. These different dynamic methods make it possible to determine the U -value but at least one day of measurement remains necessary.

The second category of method for determining wall thermal resistance involves an active approach which consists in using an artificial thermal source to create a controlled heat flux through the wall. The main objective of these methods is to allow shorter experimental times and to be less dependent on weather conditions. Sassine et al. [28] proposed an experimental set-up using a radiator fixed on a face of a box (called "heating" box) inside which the tested wall is placed. The estimated thermal resistance and heat capacity by using the thermal quadrupole approach were quite close to theoretical values, however it required a long measurement time (around 90 hours) which is similar to passive tests. Chaffar et al. [29] estimated thermal resistance and heat capacity values of a homogeneous wall by heating one face by means of a heating resistance and recording the temperature of the other face using an IR camera. A laboratory device developed in [30] allowed estimating wall thermal resistance in active mode by using infrared thermography and the thermal quadrupole model. This device is a cubic box whose front face is open and facing the investigated wall and rear face contains halogen spotlights. Several walls with internal insulation were studied in laboratory and lead to an estimated value with a margin of error within $\pm 20\%$ in comparison to the theoretical value. The authors mentioned that a measurement time of at least 1.5 hours was necessary. However, these latest studies were limited by their high sensitivity to the heat exchange coefficient. In [31], Rasooli et al. proposed an active method called "Excitation Pulse Method" (noted EPM) applying on the interior wall surface a temperature regulation whose shape was triangular and magnitude was at least 1°C . For regulating the temperature of the wall surface, a fan (for cooling) and an infrared radiative heater were equipped to deliver the thermal excitation every ten seconds. A difference of less than 2% on the thermal resistance was found for 14 days of measurement for standard method and 1.5 hour for the EPM method. In [32], the authors presented another study based on EPM and highlighted that the required test duration must be at least twice the total response time of the wall. According to the authors, their proposed method did not work well with heavily insulated walls (because of lateral effect) and cavity walls

(because of the thermal dissipation in the air). Another active method was proposed by Meulemans [33]. This approach called QUB/e method allowed measuring local U -value of building elements within one night without occupancy by heating and cooling the inside environment of a tested room by means of several heaters. The authors reached a good agreement for U -values between ISO 9869-1 and QUB/e methods. François et al. [34] proposed a similar rapid active method consisting in heating the indoor air for a few hours and in applying inverse methods (“white-box” or ARX “black-box” models) to measured surface heat fluxes and temperatures. It was validated on a full-scale wall (load bearing wall with an internal insulation system) built inside a climate chamber. Recently an active method [35] was based on a pulse shaped excitation generated by a heating resistance in contact with the wall. The acquisition of the input heat flux as well as temperatures at both the wall surface and the interfaces between tested materials enabled the estimation of characteristics of a mud-straw coating/hemp concrete assembly thanks to an inversion procedure. These results require measurement times of the order of a day.

This state of the art shows that on the one hand the passive approaches require some strict environmental conditions and quite long measurement duration and on the other hand that the active methods are not systematically applicable. In this context, a research project called RESBATI funded by the French National Research Agency was launched between several industrial and academic partners (Cerema, CERTES, CSTB, IFSTTAR recently renamed Université Gustave Eiffel, LNE and THEMACS Ingenierie). The project’s main objective is to develop an *in situ* measurement prototype based on an active approach to assess the thermal resistance of opaque walls (large surface without irregularities, such as thermal bridges or openings) that can be used whatever the wall, the type of building (occupied or not) and the environmental conditions. It is also essential that this prototype can be used before a renovation, during construction, upon delivery, and during the use of a building. Moreover this prototype should require short measurement duration (less than 12 h). Finally its installation has to be simple and fast so that professionals of the building sector can use it. The task “Study of methods robustness” of the RESBATI project has already been the subject of an article [36] presenting a numerical benchmark of different identification methods of the project partners (CERTES, CSTB, IFSTTAR) in the context of a thermal excitation of the wall and the analysis of its response in dynamic regime. This made it possible to evaluate the identification abilities of the

inverse methods (estimated value, uncertainty, calculation time) to assess the thermal resistance of opaque building walls according to the test characteristics (wall type, weather conditions, duration of the test, etc.). The work presented in this article aims to associate these identification methods with the experimental prototype developed in the RESBATI project. This prototype allows a robust and quick measurement under real conditions. By using an **instrumented** aluminum plate, the convective heat transfer coefficient is eliminated from the estimation model by using the net heat flux absorbed by the wall surface. Moreover, this metal plate helps homogenize the thermal excitation imposed on the wall surface. An extended test campaign was carried out in different climatic chambers for different environmental conditions. The walls studied during this study are among the most common in the French building stock: **Internal Insulation Wall (noted IIW)**, **External Insulation Wall (EIW)**, **Wood Frame Wall (WFW)** and **Single Concrete Wall (SCW)**.

The paper is organized as follows. The proposed measurement prototype is described in Section 2 (**experimental setup, instrumentation, identification methods, validation in the laboratory**). Then, the measurement campaign carried out is detailed in Section 3 (**tested walls, climatic chambers, environmental conditions**). In Section 4, the identification results are analyzed and discussed **to evaluate the performance of the prototype and to highlight limits and operational recommendations depending on walls and environmental conditions**. Some conclusions and **perspectives** are presented in Section 5.

2. Measurement prototype

2.1. Prototype and experimental setup

The measurement prototype is composed of two main elements: the thermal excitation source and the aluminum plate.

The thermal excitation source consists of a lamp box whose structure is made of wood and inner faces are covered by a reflective film to homogenize heat flux leaving its open front face where the tested wall is put right in front (see Fig. 1). Its backside contains a series of halogen lamps (12 V-20 W) that create the thermal excitation flux imposed on the wall surface. This box was designed in a previous research work [30]. This study allowed to determine the optimal electrical circuits to be used to obtain a heat flux density on the front face as homogeneous as possible.

The main problem encountered in this previous study was the need to know the heat transfer coefficient on the wall surface to obtain an accurate estimation of the wall thermal resistance. As this coefficient is not constant and difficult to measure *in situ* with a small uncertainty, it was necessary to estimate this coefficient by an inverse method. A sensitivity study showed that a small error on the heat exchange coefficient value can lead to huge errors on the estimation of the wall thermal resistance. Thus, it was necessary to override this problem and to find an experimental improvement of the existing device.

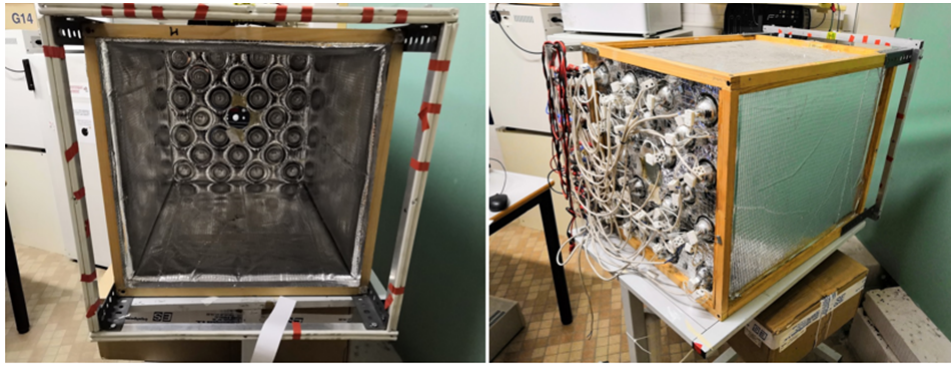


Figure 1: Front view (left) and rear view (right) of the lamp box.

The solution adopted was to add to the prototype an aluminum plate of dimension $600 \times 600 \times 5 \text{ mm}^3$. This instrumented plate constitutes the main improvement of the measurement device. It is placed **facing the lamps and in contact with the wall** (see Fig. 2). The lamp thermal excitation flux ensures the heating of this metallic plate (a black coating is used to enhance radiative absorption). This plate is highly conductive, of small thickness and in contact with the wall surface. So it behaves like a heating element on the surface of the wall. Herein, the aluminum was chosen because of its strong resistance to deformation and humidity. It ensures the repeatability of measurement under different conditions. This metal finally makes it easy to dig grooves on its surface. The lateral extension of 600 mm of the aluminum plate was chosen because it is the most common distance between metallic rails or wood studs used for fixing insulation panels on building walls (for instance when using mineral wools). A size lower than 600 mm for the aluminum plate would lead to important 3D heat diffusion in the wall thickness. The results of the numerical benchmark in [36] have confirmed that 600 mm is

an appropriate size for the excitation plate.

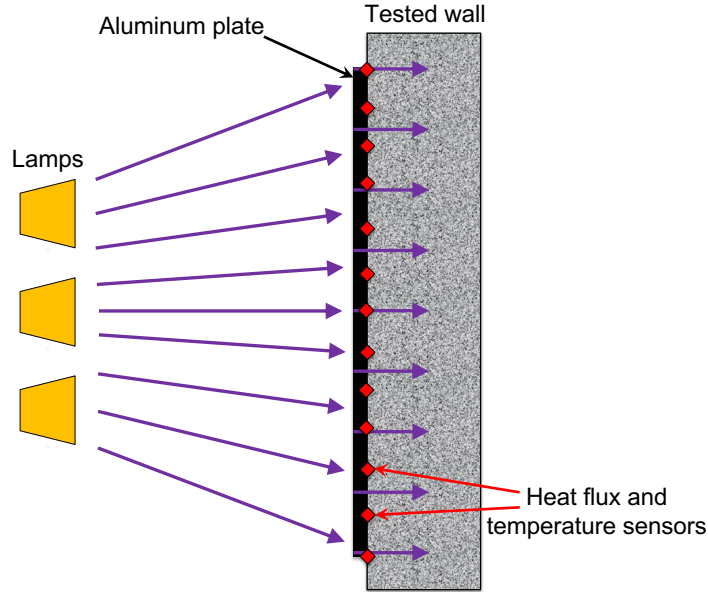


Figure 2: Heat flux transferred from the lamps to the wall surface through the aluminum plate.

On the face against the wall surface (named white side), several thermocouples and heat flux meters are installed, as shown in Fig. 3. This integration allows reducing the time of installation of the prototype on the wall. Indeed one hour was required with the previous version of prototype while it can be done in a few minutes with the new version. For the estimation of the wall thermal resistance, only the temperature and heat flux measured at the center of the plate are used. The other temperature and heat flux sensors are used to check the uniformity of the thermal excitation of the wall. The opposite surface of this plate (named black side) is painted by a black coating paint to improve the radiative absorption.

Thanks to fast thermal lateral diffusion because of the high thermal conductivity of aluminum, the plate allows homogenizing rapidly temperature and heat flux imposed on the wall surface by the white side of the plate. As presented in Fig. 4, the temperature of measurement points in the heating zone is quite uniform and there is little lateral heat loss in this area. Moreover, the black side of the plate absorbs a maximum of heat flow in the testing environment which is then homogenized and transferred to the wall surface.

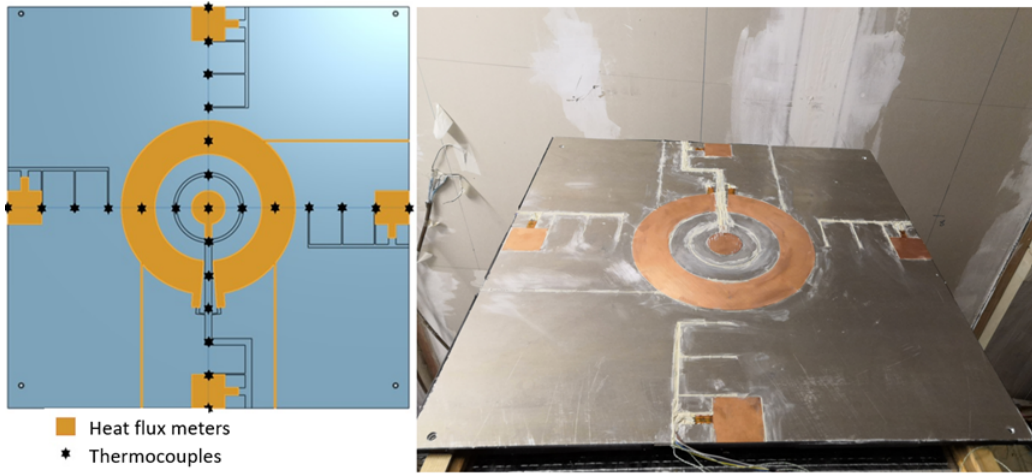


Figure 3: Sensor locations on the surface of the aluminum plate (left) and real view of the plate with the face in contact with the wall surface (right).

This prototype can therefore filter unwilling noises from small variations of the environment, what the previous prototype could not achieve. Fig. 4 also shows the noise level during an *in situ* measurement by using the heat flux meter of the prototype. It is much lower than using a heat flux meter fixed on the wall surface in contact with the air.

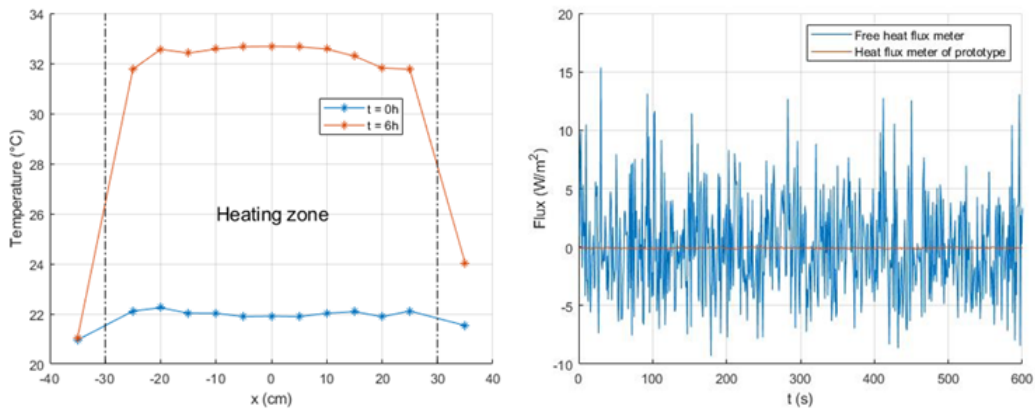


Figure 4: Horizontal temperature profiles at the beginning and after 6 hours of heating by using the aluminum plate (left) and heat flux noises measured by a heat flux meter without protection and by the circular heat flux meter at the center of the aluminum plate (right).

Note finally that a guarded insulation around the aluminum plate is strongly recommended to prevent heat losses and air leakage on the plate side surfaces. The main interest of using this plate is to directly measure the net heat flux absorbed by the wall surface instead of evaluating the incident heat flux coming from the lamps and the convection heat flux, which are very sensitive to the experiment environment. As mentioned previously, a small mistake in measuring these parameters can lead to a wrong identification result (see [37]). The complete setup of the prototype is shown in Fig. 5.

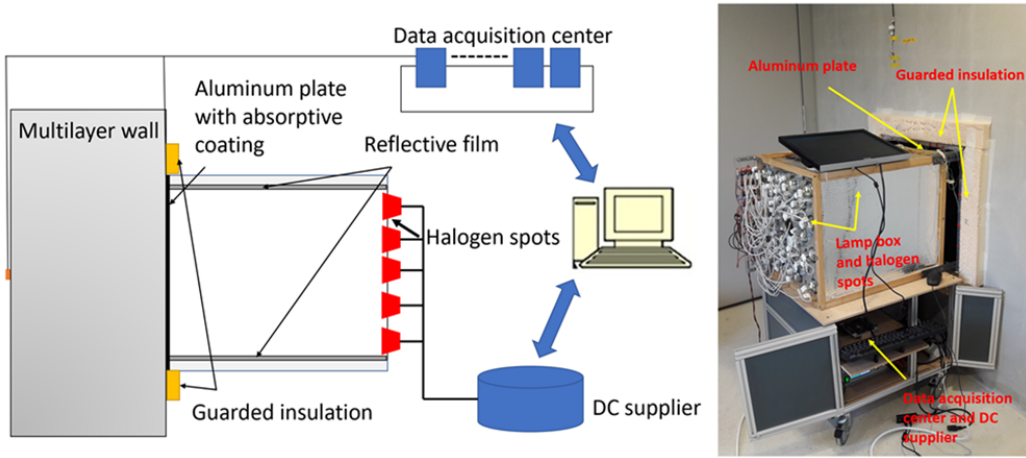


Figure 5: Schematic (left) and real (right) views of the experimental setup.

2.2. Instrumentation

The thermocouples used in this study are of type K with an operative range from -75°C to 250°C . Before integrating the sensors on the aluminum plate, all thermocouples have been calibrated by using a certificated temperature sensor PT100 (called the reference thermometer) whose error is $\pm 0.06^{\circ}\text{C}$. The procedure for calibrating thermocouples is as follows. First, all thermocouples are attached together with the reference thermometer. Then the whole is placed in a borosilicate glass beaker filled with purified water. The temperature of the water bath is controlled, varying from 0°C to 65°C by steps of 5°C . A stable temperature value is reached at each temperature step. Polynomial calibration curves are finally obtained by fitting the measurement values of each thermocouple to the reference ones. The uncertainty on temperature measured after calibration was evaluated to 0.5°C .

The heat flux meters were calibrated by the manufacturer Captec[®]. The sensitivity coefficients are 22 $\mu\text{V}/(\text{W}\cdot\text{m}^{-2})$, 44 $\mu\text{V}/(\text{W}\cdot\text{m}^{-2})$ and 205 $\mu\text{V}/(\text{W}\cdot\text{m}^{-2})$ for the square, circle and ring-shaped heat flux meters respectively. The uncertainty on heat flux meter sensitivity is equal to 3%.

All thermal sensors are connected to conditioning modules plugged into a data acquisition controller (model cDAQ-9137 from National Instruments[®]). A LabVIEW[®] application allows collecting and storing measurement data. Data files are then post-processed for the estimation of the wall thermal resistance.

2.3. Identification strategy

2.3.1. Inverse problem

With the passive method from the ISO 9869-1 standard [14], the wall thermal resistance can be calculated directly by the ratio between the temperature difference between the inner and outer wall surfaces and the heat flux. This formula is true if the considered system is in the steady-state regime. Hence, to identify the thermal resistance on a reduced time interval (less than 12 h) from transient thermal measurement, an active technique combined with inverse modelling techniques is considered herein. The wall characteristics (thermal conductivity, heat capacity, etc.) are sought to minimize a data misfit functional, *i.e.* least-square gap between the real measurement data and the model output. As a low number of sensors are used to identify many wall parameters, the inverse problem can be ill-posed. To avoid the ill-posed nature of the problem, different strategies can be considered. One can use a maximum of *a priori* information like the wall thickness, sensitivity analysis methods to limit the model updating to the most significant model parameters [38, 39, 40, 41] and regularization techniques such as Tikhonov regularization [36, 42, 43, 44] or Bayesian framework [7, 27, 36, 45, 46].

According to the numerical study in [36], only the temperature on the internal surface of the studied wall (noted T_{SI}) is considered in the inversion process. In this case, the least-squares functional $S(\beta)$ of estimated parameters β can be written as:

$$S(\beta) = \int_{t=0}^{t=t_f} \left(T_{SI}^{model}(t, \beta) - T_{SI}^{meas.}(t) \right)^2 dt \quad (1)$$

where t_f is the solicitation time of the wall, $T_{SI}^{model}(t, \beta)$ and $T_{SI}^{meas.}(t, \beta)$ are the internal surface temperatures at time t obtained from the direct model and the measurement respectively. Furthermore, the temperature of the external wall surface T_{SE} , the net heat flux absorbed by the internal wall surface ϕ_{SI} and the solar radiation ϕ_{rad} are used in the direct model as boundary conditions. Fig. 6 shows an example of measurement data obtained during a test on a **IIW** wall under natural environmental conditions.

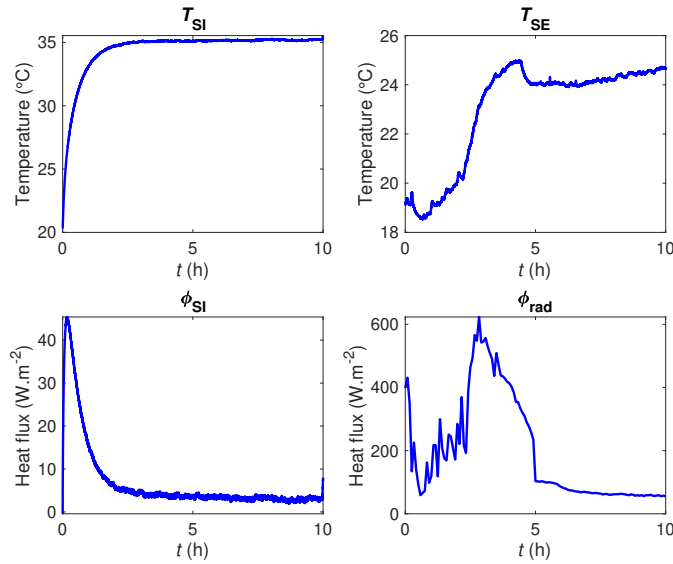


Figure 6: Example of measurement data used in the thermal resistance estimation (test on a **IIW** wall under natural environmental conditions).

2.3.2. Identification algorithms

Three research teams participated in the identification work: CERTES, CSTB and IFSTTAR. Each team has a different approach. The direct model and the identification algorithm considered by each team are summarized in Table 1. For more details, the reader can refer to [36].

2.4. Prototype validation in the laboratory

Before the climatic chamber **measurement campaign**, the prototype is tested on an **Internal Insulation Wall (IIW)** structure fixed on an interior

Table 1: Strategy of each partner for the identification of the wall thermal resistance (more details in [36]).

	Direct model	Identification algorithm	Estimated parameter
CERTES	Thermal quadrupoles in 1D	Robust Adaptive Metropolis method [47]	Thermal effusivity and time constant for each layer (4 layers)
CSTB	Equivalent RC circuit in 1D	Maximum likelihood estimation [48]	Equivalent thermal resistance and thermal capacitance for each layer (3 layers)
IFSTTAR	Heat transfer equation in 1D	Descent Gradient method with Tikhonov regularization [44]	Thermal conductivity and volumetric heat capacity for each layer by fixing its thickness (4 layers)

concrete laboratory wall. The insulation part includes two layers: a plaster-board noted BA13 (13 mm thick) and a layer of polystyrene noted PSE (80 mm thick) which result in a theoretical thermal resistance of $2.55 \text{ m}^2 \cdot \text{K} \cdot \text{W}^{-1}$ (computed from manufacturer data). This panel is fixed on a laboratory wall whose thermal resistance is around $0.3 \text{ m}^2 \cdot \text{K} \cdot \text{W}^{-1}$. The equivalent thermal resistance of the entire wall is $2.85 \text{ m}^2 \cdot \text{K} \cdot \text{W}^{-1}$ (calculated theoretical value). The structure of the investigated wall and the placement of the prototype are presented in Fig. 7. Note that the studied wall is located inside a building and is therefore not submitted to external weather conditions. Moreover, there is no environmental control during the test. The objective of this validation step is to examine the ability of the proposed prototype to estimate the resistance of such a common insulated wall using 12 hours of measurement data. Only the CERTES estimation algorithm is used in this study.

Fig. 8 shows the experimental data measured with two different heating powers (240 W and 120 W corresponding to 100% and 50% of heating power respectively). The temperature and the heat flux measured on the interior

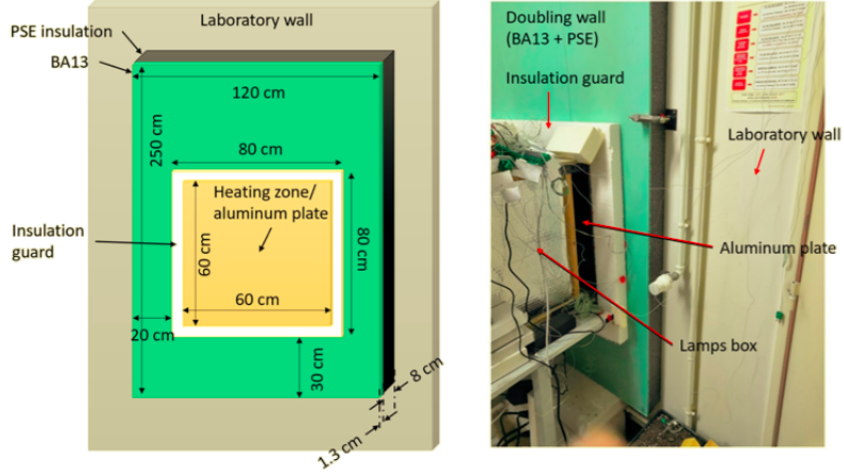


Figure 7: Validation test configuration with the measurement prototype in the laboratory.

surface heated by the prototype (noted T_{SI} and ϕ_{SI} respectively) react significantly to thermal excitation while the surface temperature T_{SE} on the other side of the wall is almost constant during the tests, which validates the assumption of constant environmental conditions. The differences observed on the external wall surface temperature T_{SE} in Fig. 8 between the two experiments (less than 0.5°C) are due to slight differences in environmental temperatures during the experiment. The active solicitation over such a short period (less than 12 h) does not affect the surface temperature on the other side.

Fig. 9 shows the ratios between estimated and theoretical thermal resistances (noted R_{estim} and R_{theo} respectively) of the tested wall for the two tests. Both cases return very accurate results with less than 2% of error compared to the theoretical value. Besides, the results of test at 100% of heating power converge faster and lead to lower uncertainties than those of test at 50%. This figure shows greater sensitivity of the identification algorithm over the first few hours for the highest heating power. However, the observed differences tend to cancel out beyond 6 hours of measurement (estimated thermal resistances and uncertainty values almost identical). In conclusion, 6-hour measurement data with the maximum heating power seem to be a good compromise in terms of precision, uncertainty and measurement time to estimate the thermal resistance of this wall under laboratory conditions.

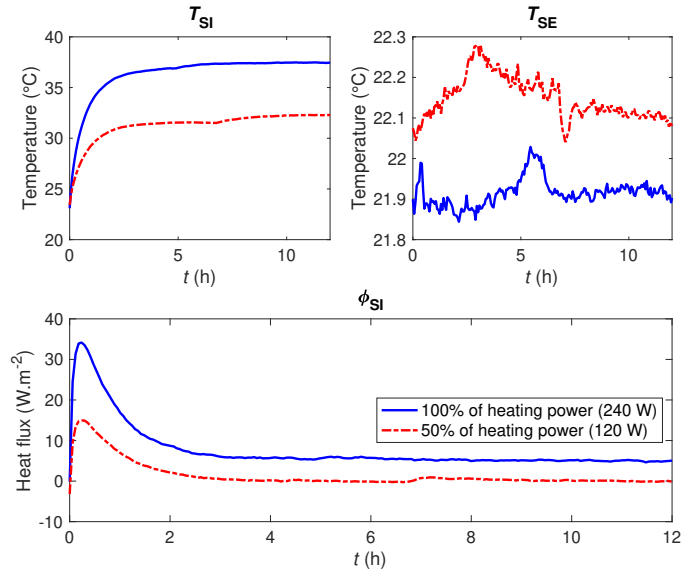


Figure 8: Measurement data during the prototype validation tests in the laboratory under two levels of heating power.

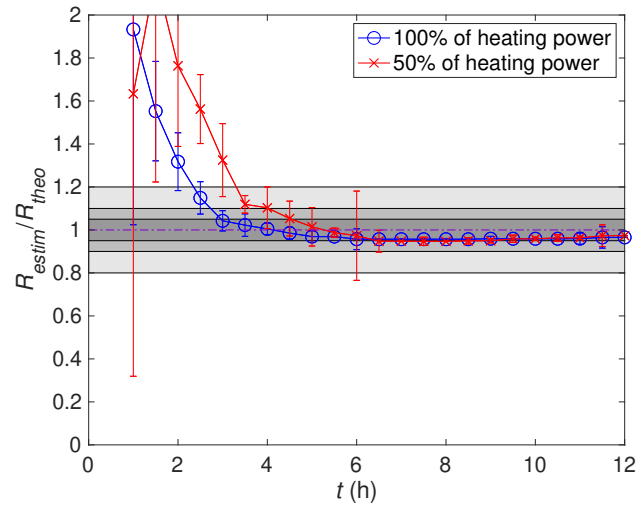


Figure 9: Estimated thermal resistance normalized by the theoretical value for the prototype validation in the laboratory under two levels of heating power by using CERTES estimation algorithm.

3. Investigated walls and climatic chamber tests

3.1. Case studies

3.1.1. Tested walls

First three walls of dimension $2 \times 2 \text{ m}^2$ were specifically built for the research project RESBATI to be transportable to the different sites listed in Section 3.1.2 in order to conduct various types of tests. These tested walls are: Internal Insulation Wall (IIW), External Insulation Wall (EIW) and Wood Frame Wall (WFW). The insulation layer is on the internal side for the IIW while this layer is close to the external side in the case of the EIW. The WFW has the most complicated structure with several vertical and horizontal wood frames and the highest thermal resistance. Lastly, a Single Concrete Wall (SCW) located in a real building and composed of a single layer of concrete represents the simplest non insulated wall. The details of each wall are given in Table 2.

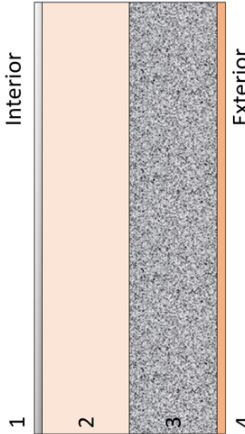
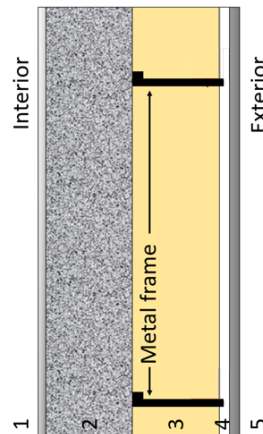
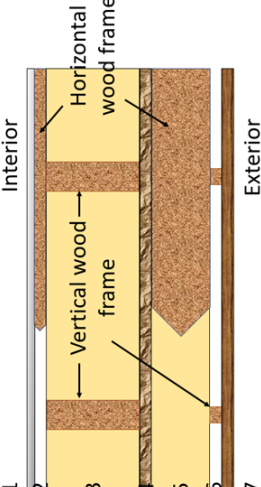
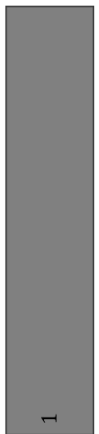
Theoretical thermal resistances noted R_{theo} indicated in this table are calculated from the composition of each layer constituting the wall. The thickness values (noted e) were measured by CSTB during manufacturing for IIW, EIW and WFW or assumed to be known for SCW. The thermal conductivity values (noted λ) were determined by the Guarded Hot Plate device [49] at LNE or the Hot Disk device [50] at Cerema at 10°C or come from the French thermal regulation [2] or ISO 6946 [22] (to deduce equivalent thermal conductivities of the air gaps from the thermal resistance given by this standard).

3.1.2. Climatic chambers

In this study, three climatic chambers are used to test the four real-scale walls under controlled and natural conditions.

The first one is the energy room at LNE which corresponds to a climatic chamber inside another climatic chamber. It is composed of an internal cell with the dimensions of a dwelling (3.42 m of side on 2.29 m high, surface of the test specimen 7.83 m^2). The latter is surrounded by 4 climatic chambers in which it is possible to modify the temperature between -7°C and 35°C . The four surrounding boxes (front cell, guard, floor and ceiling) can be controlled separately. The internal cell named REBECCA (Research and Testing of Buildings and Heat Emitters under Artificial Climate) has been built to reproduce the principle of a guarded hot box test but with more space inside to install additional devices. The front panel was equipped with the wall

Table 2: Description of the four tested walls: geometries, thermophysical properties of materials and theoretical thermal resistances (*: duralumin, **: equivalent thermal conductivity computed from the thickness of the air gap and the thermal resistance from [22]).

Wall name and dimensions	Structure (horizontal cross section)	Layer	Material	e (m)	λ (W/m.K)	R_{theo} ($m^2 \cdot K/W$)
Internal Insulation Wall (IIW) - $2 \times 2 \text{ m}^2$ - 0.298 m thick		1	Plasterboard	0.013	0.25 [2]	4.02
		2	Expanded polystyrene	0.12	0.032 [49]	
		3	Building block	0.15	0.74 [50]	
		4	External coating	0.015	0.94 [50]	
External Insulation Wall (EIW) - $2 \times 2 \text{ m}^2$ - 0.326 m thick - 600 mm between metal frames		1	Plasterboard	0.013	0.25 [2]	Without metal frame: 3.86 With metal frame: 2.11
		2	Building block	0.15	0.74 [50]	
		3	Stone wool insulation	0.12	0.035 [49]	
		4	Air gap	0.04	0.22 [22]**	
		5	Metal cladding*	0.003	160 [2]	
Wood Frame Wall (WFW) - $2 \times 2 \text{ m}^2$ - 0.354 m thick - 600 mm between vertical wood frames (widths: 45 mm and 20 mm)		1	Plasterboard	0.013	0.25 [2]	Without wood frame: 9.11 With wood frame: 2.03
		2	Air gap	0.02	0.11 [22]**	
		3	Glass wool insulation	0.16	0.031 [49]	
		4	OSB sheathing	0.02	0.13 [2]	
		5	Glass wool insulation	0.1	0.031 [49]	
		6	Air gap	0.02	0.11 [22]**	
		7	Wood siding	0.021	0.13 [2]	
Single Concrete Wall (SCW) - $10 \times 3 \text{ m}^2$ - 0.2 m thick		1	Concrete	0.2	1.4 [2]	0.14

to be studied. In order to ensure that the entire heat flow passes through the tested wall, the 5 walls of the inner cell in contact with the thermal guard have been insulated with Vacuum Insulated Panels having a thermal resistance greater than $10 \text{ m}^2 \cdot \text{K} \cdot \text{W}^{-1}$. The test can be carried out under steady-state conditions without solar radiation.

The second climatic chamber at Cerema is equipped with two refrigeration circuits. The available test volume can be separated into two distinct and thermally independent parts. Hence, the tested wall was placed at the interface of the two parts and it was studied according to different thermal configurations: in constant or variable conditions. Moreover, it is possible to put the external side of the studied wall in contact with the external natural environment, which enables solar radiation.

The last one is the Sense-City equipment at Université Gustave Eiffel-IFSTTAR which is illustrated in Fig. 10. It is made of a 3200 m^3 climatic chamber and two instrumented full-scale urban areas of 400 m^2 each ($20 \text{ m} \times 20 \text{ m}$). The climatic chamber provides a controlled environment and is mounted on rails in order to move from one urban area to the other. Using the climatic chamber, we can replicate controlled weather conditions with temperature ranging from -10°C to 40°C , humidity ranging from 20% to 95%, rain events, sun exposure and air pollution. By removing the climatic chamber, natural weather conditions can be considered. The first urban area includes a wooden house, a small house made of bio-based materials, a two-story precast concrete building and a street network including sidewalk, street lighting, crosswalk and traffic light. In this paper, we will focus in this climatic chamber on the wall of the concrete building (**SCW**).



Figure 10: Sense-City equipment: urban area #1 of 400 m^2 inside the climatic chamber (left) and outside the climatic chamber (right).

3.1.3. Testing conditions of the measurement campaign in climatic chambers

The studied walls are tested under different constant, variable and natural environmental conditions in the climatic chambers (see Table 3). **Let us underline that for practical and technical reasons, the considered walls were not tested in all laboratories under all test conditions.** Under constant conditions, both internal and external environments are maintained constant by the climatic chamber which is switched on at least 12 hours before each test to ensure the steady-state regime. Under variable conditions, the internal environment is maintained constant while an external air temperature profile is applied on the external side of the tested wall. Under natural conditions, the external side is subject to an outdoor environment including solar radiation. Tables 4 to 7 detail the characteristics of each test for each wall studied, including the heating power of the lamp box, the internal and external environmental conditions and the solar radiation.

Table 3: Tested walls and their corresponding environmental conditions by using the three climatic chambers.

Chamber	Condition			Tested wall
	Constant	Variable	Natural	
LNE	×			IIW, EIW, WFW
Cerema	×	×	×	IIW
IFSTTAR	×	×	×	SCW

Fig. 11 and 12 show the external air temperature T_e and solar radiation ϕ_{rad} for the variable and natural cases respectively (only **IIW** and **SCW** are subject to these types of conditions).

Tests in variable conditions give an average external air temperature lower than the internal air temperature of 20°C, except **IIW** tests 17 and 18 (T-Var. 5) for which the external air temperature is higher than the internal air temperature. The solar radiation profile S-Var. 1 only concerns the **SCW** tests 40 and 41 (no solar radiation is applied for the other tests in variable conditions) and was obtained by using the sun lights placed at the ceiling of the climatic chamber Sense-City. The different solar radiation profiles were measured using a pyranometer.

In the **IIW** cases under natural conditions, two different measurements are launched: without solar protection (tests 19 and 20) and with (tests 21 and 22) as shown in Fig. 13. **The lateral dimensions of the solar protection (60×60 cm²) correspond to the size of the aluminum plate and makes it pos-**

Table 4: Detailed conditions of the tests in climatic chambers on the **Internal Insulation Wall (IIW)**.

Wall	Test case	Heating power	Interior	Exterior	Solar radiation
IIW	3	240 W	20°C	0°C	0
	4	120 W	20°C	0°C	0
	5	240 W	30°C	10°C	0
	6	120 W	30°C	10°C	0
	7	240 W	25°C	35°C	0
	8	120 W	25°C	35°C	0
	9	240 W	20°C	T-Var. 1	0
	10	120 W	20°C	T-Var. 1	0
	11	240 W	20°C	T-Var. 2	0
	12	120 W	20°C	T-Var. 2	0
	13	240 W	20°C	T-Var. 3	0
	14	120 W	20°C	T-Var. 3	0
	15	240 W	20°C	T-Var. 4	0
	16	120 W	20°C	T-Var. 4	0
	17	240 W	20°C	T-Var. 5	0
	18	120 W	20°C	T-Var. 5	0
	19	240 W	20°C	T-Nat. 1	S-Nat. 1 without solar protection
	20	120 W	20°C	T-Nat. 2	S-Nat. 2 without solar protection
	21	240 W	20°C	T-Nat. 3	S-Nat. 3 with solar protection
	22	120 W	20°C	T-Nat. 4	S-Nat. 4 with solar protection

sible to obtain a good compromise between a reasonable size and a significant limitation of the impact of the solar radiation in the center of the measurement zone. These four tests are conducted during the daytime in August 2020. Besides, both two **SCW** tests under natural conditions are launched during the daytime in February 2020 without solar protection (tests 42 and 43).

Regarding the measurements on the **EIW**, only tests 23 and 24 are performed on the internal surface of the wall (the reason will be provided later). When testing outside, the prototype is installed on the external metal siding

Table 5: Detailed conditions of the tests in climatic chambers on the **External Insulation Wall (EIW)**.

Wall	Test case	Heating power	Interior	Exterior	Solar radiation
EIW	23	240 W	30°C	15°C	0
	24	120 W	30°C	15°C	0
	25	240 W	25°C	15°C	0
	26	240 W	25°C	15°C	0
	27	120 W	25°C	15°C	0
	28	240 W	20°C	20°C	0
	29	120 W	20°C	20°C	0
	30	240 W	20°C	30°C	0
	31	120 W	20°C	30°C	0
	32	240 W	20°C	15°C	0
	33	120 W	20°C	15°C	0

Table 6: Detailed conditions of the tests in climatic chambers on the **Single Concrete Wall (SCW)**.

Wall	Test case	Heating power	Interior	Exterior	Solar radiation
SCW	34	240 W	20°C	20°C	0
	35	120 W	20°C	20°C	0
	36	240 W	20°C	5°C	0
	37	120 W	20°C	5°C	0
	38	120 W	20°C	T-Var. 6	0
	39	120 W	20°C	T-Var. 6	0
	40	120 W	20°C	T-Var. 6	S-Var. 1 without solar protection
	41	120 W	20°C	T-Var. 6	S-Var. 1 without solar protection
	42	120 W	20°C	T-Nat. 5	S-Nat. 5 without solar protection
	43	120 W	20°C	T-Nat. 6	S-Nat. 6 without solar protection

in test 25 and on the insulation layer (the metal siding is removed) for the remaining tests. For tests 25 to 33, the identifications are performed using the thermal states of the external side (T_{SE} , ϕ_{SE}) instead of those of the internal side (T_{SI} , ϕ_{SI}).

Table 7: Detailed conditions of the tests in climatic chambers on the Wood Frame Wall (WFW).

Wall	Test case	Heating power	Interior	Exterior	Solar radiation
WFW	44	240 W	20°C	0°C	0
	45	120 W	20°C	0°C	0
	46	240 W	20°C	0°C	0
	47	240 W	30°C	10°C	0
	48	240 W	25°C	35°C	0

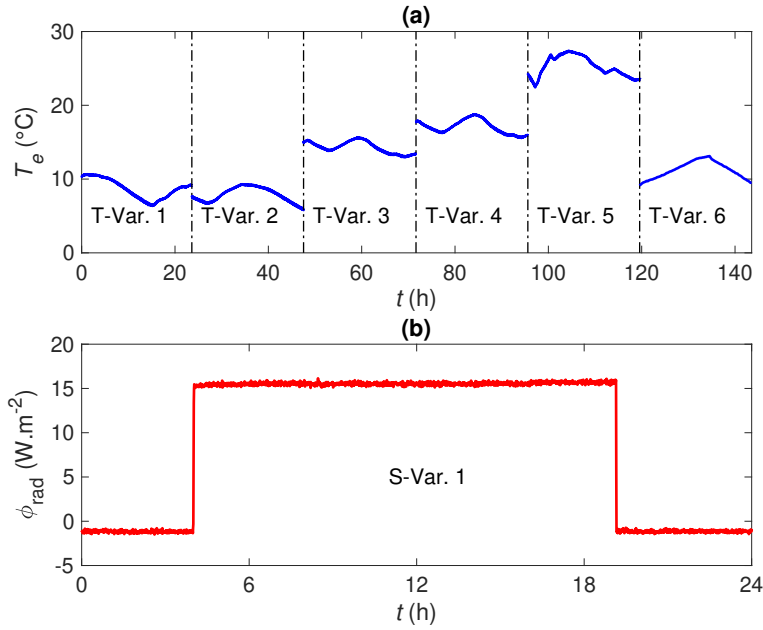


Figure 11: Variable conditions: (a) External air temperature, (b) Solar radiation.

The first two tests on the WFW (tests 44 and 45) are conducted on a zone containing thermal bridges (see Fig. 14). Another zone without thermal bridge is chosen for carrying out the other cases.

3.2. Reference values of thermal resistance of the tested walls

The theoretical thermal resistance values calculated in Section 3.1.1 are obtained assuming a perfect knowledge of the thermal properties of materials, the absence of defect or irregularities and a perfect contact between the layers.

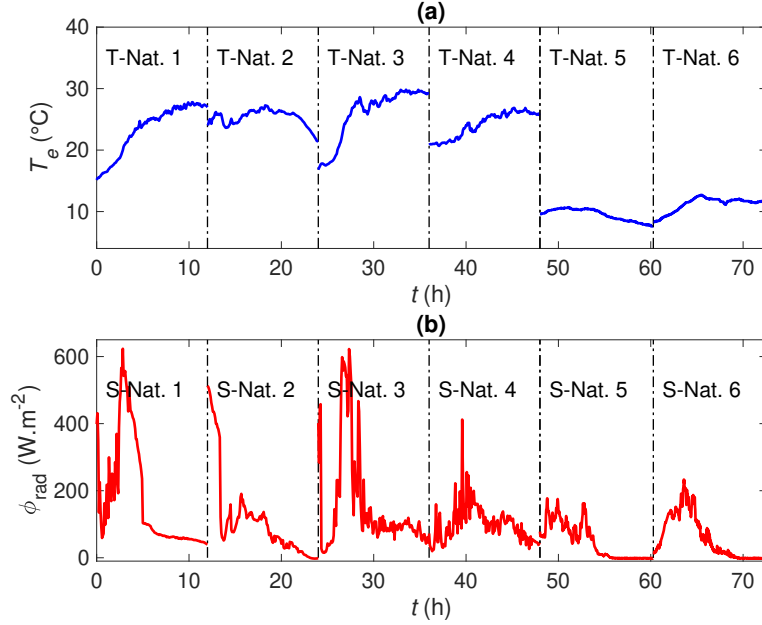


Figure 12: Natural conditions: (a) External air temperature, (b) Solar radiation.

However, manufacturer data may be imprecise and manufacturing errors are common. This is the "performance gap" discussed in several references [51, 52]. The thermal resistances of the studied walls must therefore be measured by standard passive methods, *i.e.* ISO 8990 or Guarded Hot Box (GHB) method [13] and ISO 9869-1 or Heat Flow Meter (HFM) method [14], to get reference values.

Guarded Hot Box device at CSTB [53] is used for the **IIW**, **EIW** and **WFW** because the dimensions of the walls fit the size of the device. Only the thermal resistance of the **SCW** is evaluated by the Heat Flow Meter method because this wall is located in a real building.

Table 8 presents the reference values of thermal resistance (noted R_{ref}) obtained with **these methods** and the corresponding uncertainties (noted $u_{R_{ref}}$). Three levels of operating temperature for **IIW**, **EIW** and **WFW** are tested with the GHB device because of the variation of material thermal conductivity as a function of temperature. All thermal resistance values with this method are smaller than the theoretical ones in Table 2 (without metal or wood frame for **EIW** and **WFW** respectively). In particular, the

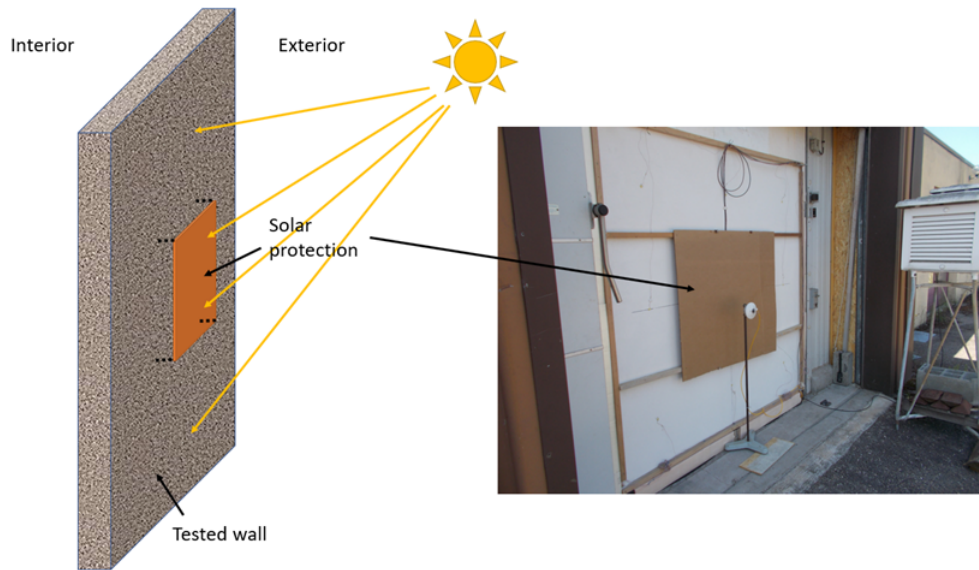


Figure 13: Solar protection of $60 \times 60 \text{ cm}^2$ used for **IIW** tests 21 and 22 under natural conditions.

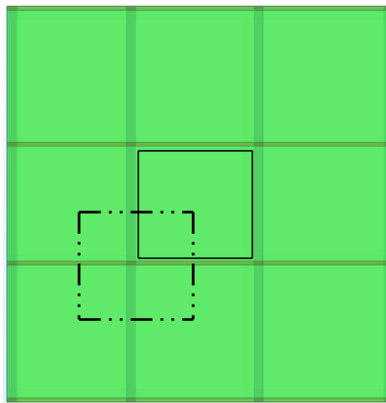


Figure 14: Measurement zones for the WFW tests with thermal bridges (dash-dotted line) and without (solid line).

EIW thermal resistances in Table 8 are much lower than the theoretical value calculated not taking into account the metal frames. Indeed the GHB measurement evaluates the thermal resistance of the wall by heating the entire wall surface ($2 \times 2 \text{ m}^2$ in this case) so as to take into account the metal frames located in the insulation layer which absorb more heat than the insulation.

Besides, the **SCW** thermal resistance is evaluated under natural conditions in Sense-City equipment by the Heat Flow Meter method. Ten days of measurement data are considered (see Fig. 15). Using the average calculation proposed in ISO 9869-1 standard, a R_{ref} value of $0.25 \text{ m}^2.\text{K}.\text{W}^{-1}$ is obtained for the **SCW** thermal resistance. This value is quite higher than that calculated theoretically in Table 2, this may be due to a conductivity resulting from [2] too high and an inappropriate supposedly known thickness.

Table 8: Reference values of thermal resistance for the four tested walls (IIW, EIW, WFW and SCW) obtained by the Guarded Hot Box (GHB) method or the Heat Flow Meter (HFM) method and corresponding uncertainties.

Wall	Standard method	Operating temperature ($^{\circ}\text{C}$)	R_{ref} ($\text{m}^2.\text{K}.\text{W}^{-1}$)	$u_{R_{ref}}$ ($\text{m}^2.\text{K}.\text{W}^{-1}$)
IIW	GHB	10	3.8	0.6
		20	3.5	0.8
		30	3.3	0.5
EIW	GHB	10	2.1	0.3
		20	2.1	0.3
		30	1.8	0.2
WFW	GHB	10	7.6	1.8
		20	7.1	1.6
		30	6.7	1.5
SCW	HFM	Ambient temperature	0.25	-

All the thermal resistance values obtained in this part come from standard measurements, unlike those in Section 3.1.1 which are partly derived from calculations. To validate the identification results, the estimation obtained with the proposed measurement prototype will be compared to the reference values presented in this section.

4. Results and discussions

In the following section, the measurement prototype and the inverse techniques presented in Section 2 are applied to the wall typologies under controlled and natural climatic conditions presented in Section 3. The estimated values of thermal resistance (noted R_{estim}) are presented and analyzed.

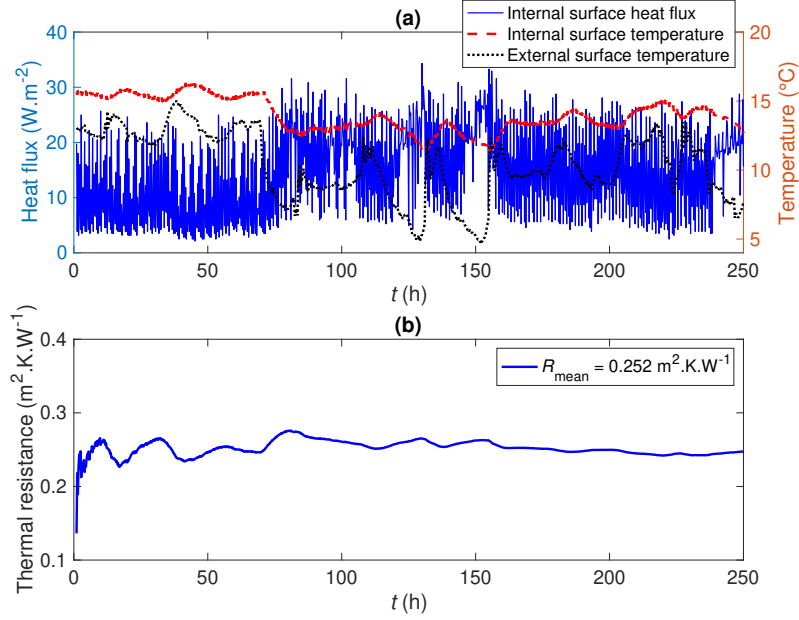


Figure 15: HFM method applied to the SCW: (a) Measurement data, (b) Computed thermal resistance.

4.1. IIW results

4.1.1. Constant conditions

The measurement data (interior and exterior surface temperatures T_{SI} and T_{SE} and interior surface heat flux ϕ_{SI} measured with the prototype) obtained under constant conditions on the IIW are presented in Fig. 16. Temperature and heat flux on the internal surface reached stable levels quite quickly (after a few hours of heating) due to the presence of the insulation layer on the measurement prototype side. Table 9 and Fig. 17 show the 6-hour estimation results obtained by using the three proposed identification algorithms presented in Table 1 and the corresponding reference values of the IIW thermal resistance (these values are taken from Table 8 by considering the average between internal and external air temperatures of each test, see Table 4).

Accurate results are obtained for all the methods in tests 3 to 6 where the internal air temperature T_i is higher than in the exterior T_e . When considering an outdoor temperature higher than the indoor temperature (tests

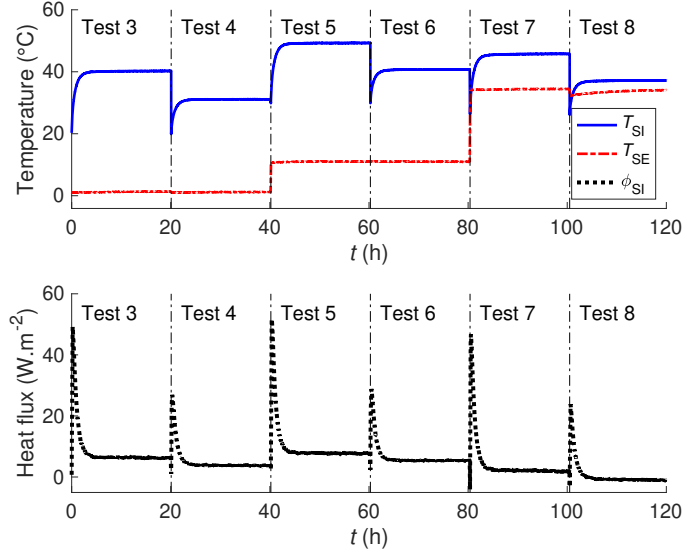


Figure 16: Measurement data of the **IIW** tests 3 to 8 under constant conditions.

Table 9: Estimated thermal resistances and corresponding uncertainties by using 6-hour measurement data for the tests on the **IIW** under constant conditions (in $\text{m}^2 \cdot \text{K} \cdot \text{W}^{-1}$) - * IFSTTAR uncertainty value only allows to derive the lowest bound of the estimated thermal resistance.

Test	R_{theo}	R_{ref}	$R_{estim} (u_{R_{estim}})$		
			CERTES	CSTB	IFSTTAR*
3	4.02	3.8	3.62 (0.03)	3.56 (0.04)	3.98 (0.84)
4	4.02	3.8	4.16 (0.03)	3.80 (0.01)	4.01 (1.13)
5	4.02	3.5	3.64 (0.04)	3.45 (0.04)	3.85 (1.41)
6	4.02	3.5	3.49 (0.30)	3.47 (0.01)	3.84 (1.42)
7	4.02	3.3	3.39 (0.03)	2.76 (0.03)	3.82 (1.09)
8	4.02	3.3	4.57 (0.04)	3.90 (0.11)	4.00 (1.19)

7-8), results are different for the 3 inverse techniques. The identified results for CSTB and IFSTTAR are slightly degraded for these tests (20% error for both methods) compared to tests 3 to 6 (5% error for CSTB and 10% error for IFSTTAR). The difference in heating power between tests 7 and 8 does not seem to have a particular influence on these identification techniques. CSTB algorithm gives overall more precise identification results

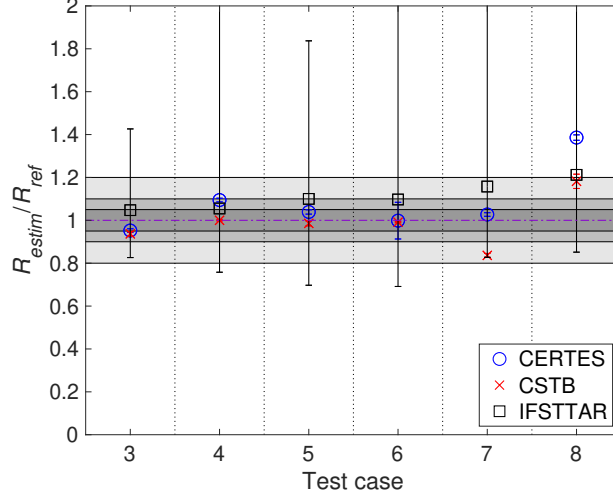


Figure 17: Estimated thermal resistances normalized by the reference value for the **IIW** tests under constant conditions by using 6-hour measurement data.

compared to IFSTTAR but the IFSTTAR technique provides an uncertainty value that allows a robust estimation of the lowest value of the thermal resistance ($R_{IFSTTAR}^{low} < R_{ref}$) in all tests: error between 15% and 30% - recalling that the reference value of the thermal resistance in GHB is determined with an error of 15%. The estimated thermal resistance with CERTES method is not well-identified only in test 8 for which $T_e > T_i$ and the heating power is at 50%. CERTES technique may be more sensitive to the heating power in tests 7-8 where the direction of the steady-state heat flux is inverse compared with the first four tests 3 to 6.

4.1.2. Variable conditions

Let us now examine the **IIW** results under variable conditions. Firstly, as explained in Table 4, we considered in tests 9 to 18 variable outdoor temperature, constant indoor temperature and no solar radiation on the outside face of the wall. The variation of the external environment observed in Fig. 18 does not influence the temperature and the heat flux on the interior surface, even with the "hot" external environment (tests 17 and 18).

According to the results presented in Table 10 and Fig. 19, the proposed

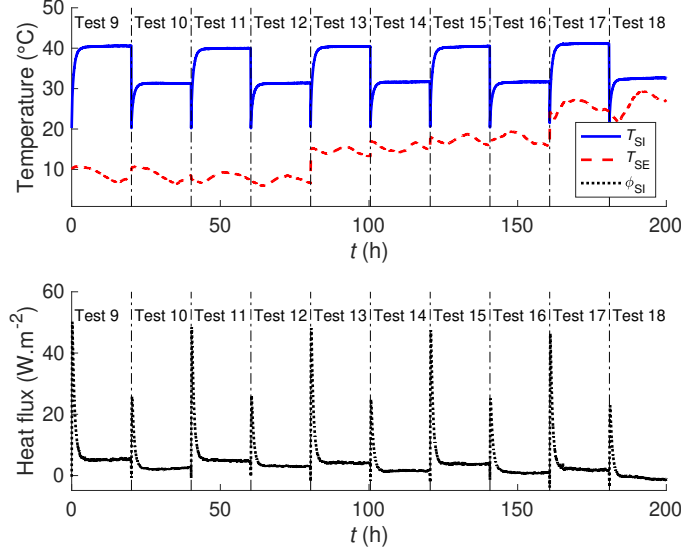


Figure 18: Measurement data of the **IIW** tests 9 to 18 under variable conditions.

prototype with the different identification techniques can provide a thermal resistance value close to the one resulting from the standard method after 6 hours of measurement for all these tests. The identified thermal resistance is globally obtained with an error of less than 10% for CSTB and CERTES (resp. less than 20% for IFSTTAR). **Nevertheless, contrary to the two other inverse techniques, IFSTTAR method still gives a robust estimation of the minimal value of the thermal resistance, i.e. $R_{IFSTTAR}^{low} < R_{ref}$ for all the test cases.** No influence of the heating power and of the variation of the outdoor temperature on the identification results appears for these tests.

4.1.3. Natural conditions

After running measurements in the climatic chamber, the external side of the **IIW** is now exposed to natural outdoor conditions. At first no protection is used on the external side of the **IIW** (tests 19-20). Then a solar protection is added for tests 21-22. The environmental condition in the interior is maintained at 20°C. The measurement data of these tests can be seen in Fig. 20. It should be noted here that when using the climatic chamber in natural mode at Cerema, the evaporator is regulated two times a day so that

Table 10: Estimated thermal resistances and corresponding uncertainties by using 6-hour measurement data for the **IIW** tests under variable conditions (in $\text{m}^2\cdot\text{K}\cdot\text{W}^{-1}$, * obtained by linear regression) - ** IFSTTAR uncertainty value only allows to derive the lowest bound of the estimated thermal resistance.

Wall	Test	R_{theo}	R_{ref}	$R_{estim} (u_{Restim})$		
				CERTES	CSTB	IFSTTAR**
IIW	9	4.02	3.67*	3.69 (0.01)	3.54 (0.02)	4.18 (0.57)
	10	4.02	3.67*	3.79 (0.08)	3.71 (0.01)	3.96 (1.15)
	11	4.02	3.7*	3.48 (0.14)	3.46 (0.05)	3.94 (0.86)
	12	4.02	3.68*	3.61 (0.01)	3.61 (0.01)	3.82 (1.24)
	13	4.02	3.58*	3.35 (0.05)	3.33 (0.06)	3.96 (0.76)
	14	4.02	3.58*	3.92 (0.01)	3.72 (0.10)	3.88 (1.18)
	15	4.02	3.53*	3.44 (0.01)	3.31 (0.08)	3.82 (0.65)
	16	4.02	3.54*	3.74 (0.01)	3.52 (0.02)	4.09 (1.19)
	17	4.02	3.45*	3.11 (0.47)	2.98 (0.08)	3.84 (0.96)
18	4.02	3.45*	3.50 (0.03)	3.31 (0.06)	3.76 (1.22)	

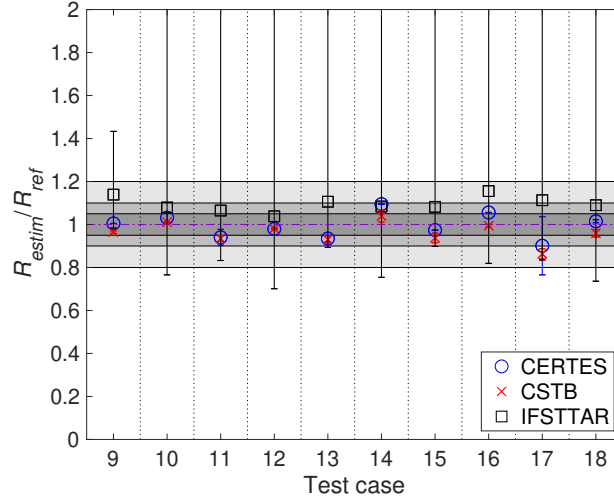


Figure 19: Estimated thermal resistances normalized by the reference value for the **IIW** tests under variable conditions by using 6-hour measurement data.

a sudden change in the measurement data is observed for all four tests.

The estimation results of these tests are presented in Table 11 and Fig.

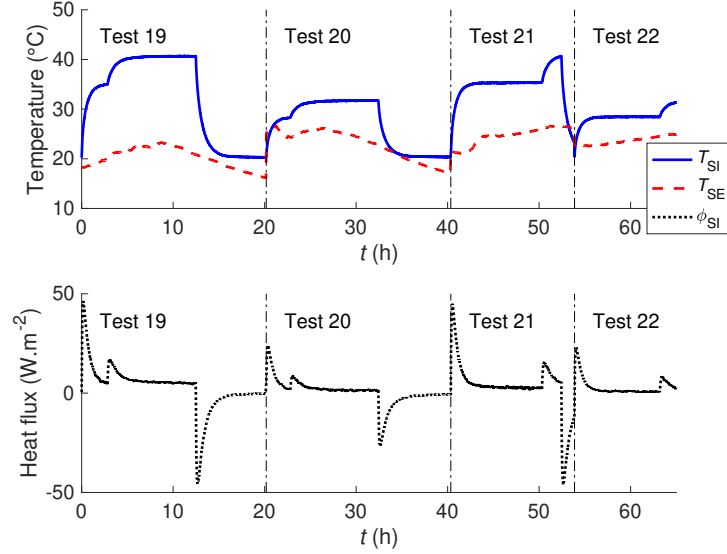


Figure 20: Measurement data of the **IIW** tests 19 to 22 under natural conditions.

21. According to these results, the influence of solar radiation on the identification results is remarkable for CERTES and IFSTTAR methods. The results of tests 19-20 without solar protection are strongly degraded for these two methods compared to those of the previous tests, especially for test 20 for which the heating power is the lowest. These unsatisfactory estimation results have their origin in the influence of solar radiation. The observation of Fig. 12 shows that the solar radiation measured on the external surface of the tested wall is much higher than the excitation heat flux shown in Fig. 20. It can be considered as a second thermal source supplying heat from the exterior. Therefore, it directly disturbs the thermal diffusion inside the wall. CERTES method is the most sensitive to solar radiation since the use of solar protection in tests 21-22 allows to get accurate identification results with this method (error less than 5%). For all these tests, the gap between the IFSTTAR deterministic thermal resistance and the reference value is less than 30%. Using IFSTTAR technique the estimation of the minimum thermal resistance of the wall remains acceptable. Finally, the CSTB method is the least affected by solar radiation since, depending on the heating power, the results obtained with solar protection are not necessarily better than without protection.

Table 11: Estimated thermal resistances and corresponding uncertainties by using 6-hour measurement data for the **IIW** tests under natural conditions (in $\text{m}^2\cdot\text{K}\cdot\text{W}^{-1}$, * obtained by linear regression) - ** IFSTTAR uncertainty value only allows to derive the lowest bound of the estimated thermal resistance.

Wall	Test	R_{theo}	R_{ref}	$R_{estim} (u_{R_{estim}})$		
				CERTES	CSTB	IFSTTAR**
IIW	19	4.02	3.45*	6.03 (0.01)	2.62 (0.24)	4.08 (0.82)
	20	4.02	3.45*	10.41 (1.91)	3.31 (0.17)	4.55 (2.60)
	21	4.02	3.45*	3.42 (0.06)	3.02 (0.03)	4.32 (0.68)
	22	4.02	3.45*	3.33 (0.06)	3.04 (0.02)	3.96 (1.08)

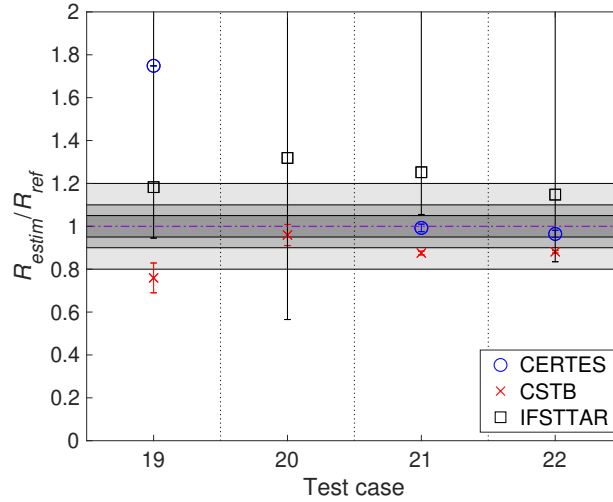


Figure 21: Estimated thermal resistances normalized by the reference value for the **IIW** tests under natural conditions by using 6-hour measurement data.

To sum up, the measurement prototype with the associated identification techniques is able to properly determine the thermal resistance of a **IIW** using 6-hour observation time in the different conditions: constant, variable and natural. In natural conditions, it is recommended to place a small solar protection on the outside face of the wall to improve the quality of the identification results.

4.2. *EIW* results under constant conditions

In the original experimental setup, an active solicitation on the interior face of the wall is proposed. Using the interior face temperature response

made it possible to properly identify the wall thermal resistance for **IIW** which has its insulation on the inside. The **EIW** type is a particular case because its insulation layer is located on the exterior side **and the thermal excitation takes place on the side of the concrete layer**. It means that the thermal excitation heat flux will diffuse from the interior face through the concrete layer before reaching the insulation. According to the numerical simulation results in Fig. 22 obtained with COMSOL Multiphysics[®], the concrete layer diffuses most of the heat flux laterally which implies that the 1D direct model used in the estimation algorithms is no longer correct. Moreover, due to this lateral diffusion, a very small amount of heat flux can reach the insulation layer so that 93% of the thermal resistance of this wall is impossible to evaluate if using the prototype on the internal surface. **Let us underline two other particularly important issues that make thermal excitation on the side of the building block unsuitable: the huge thermal capacity of the concrete layer and the need for a long measurement period to achieve a steady-state regime.**

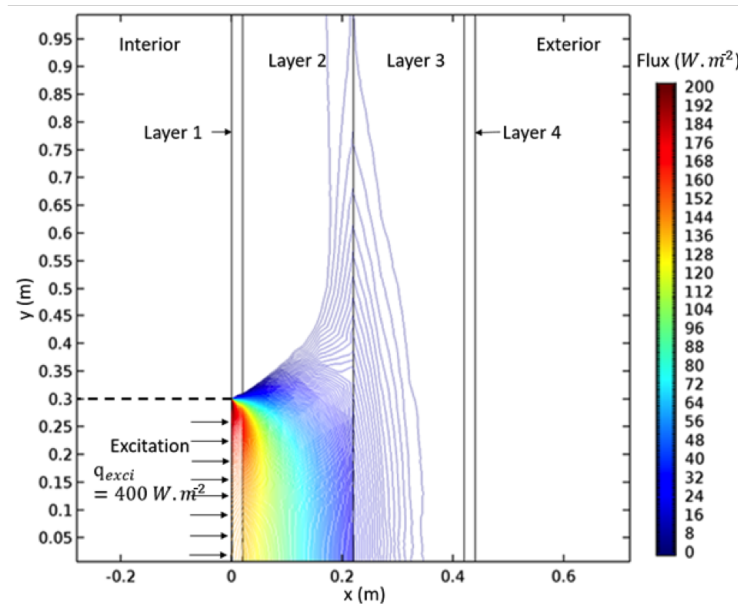


Figure 22: Heat flux isolines in the **EIW** after 24 hours of heating simulated by COMSOL Multiphysics[®] - Layer 2: concrete, Layer 3: insulation.

The measurement data of the tests 23 to 25 are shown in Fig. 23. On the one hand, unlike the **IIW** cases, the data profiles of the first two tests

23-24, for which the thermal excitation was performed directly on the internal surface of the tested wall, do not reach stable levels due to the lack of internal insulation. It means that the tested wall continues to absorb and diffuse the excitation heat flux through the concrete layer. On the other hand, test 25 with active solicitation performed on the external metal siding shows very stable thermal states. However, this quick evolution indicates that no thermal storage occurs and that the unventilated air gap between the metal cladding and the insulation diffuses 100% of the incoming heat flux. Besides, as observed in Fig. 24, by removing the metal siding for the tests 26 to 33 and installing the prototype directly on the outside insulation surface between two metal frames so that the testing zone is homogeneous, this wall becomes similar to the **IIW** case, with the same temperature evolutions for the heating surface.

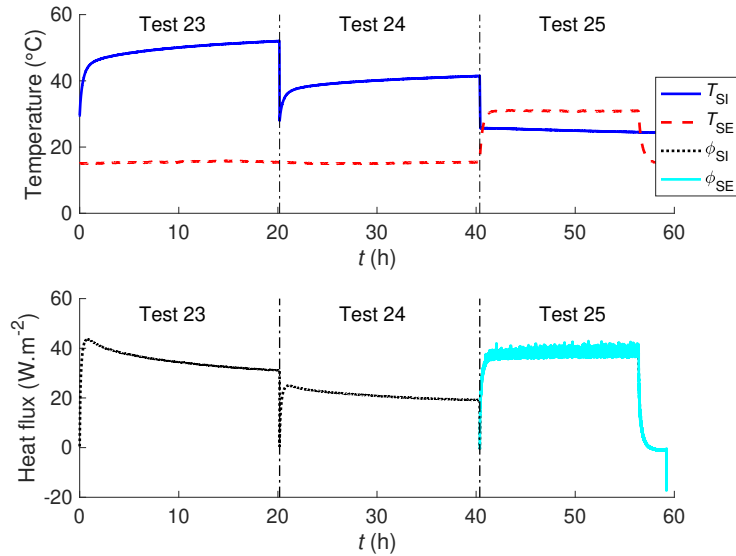


Figure 23: Measurement data of the **EIW** tests 23 to 25 under constant conditions.

Table 12 and Fig. 25 present the estimated results with 10-hour measurement data for the tests on this wall. As predicted by the numerical simulation, all identification methods fail to estimate the wall thermal resistance for the first two tests 23-24 on the internal surface. It confirms that testing on the internal surface of the **EIW** is not a good choice to estimate

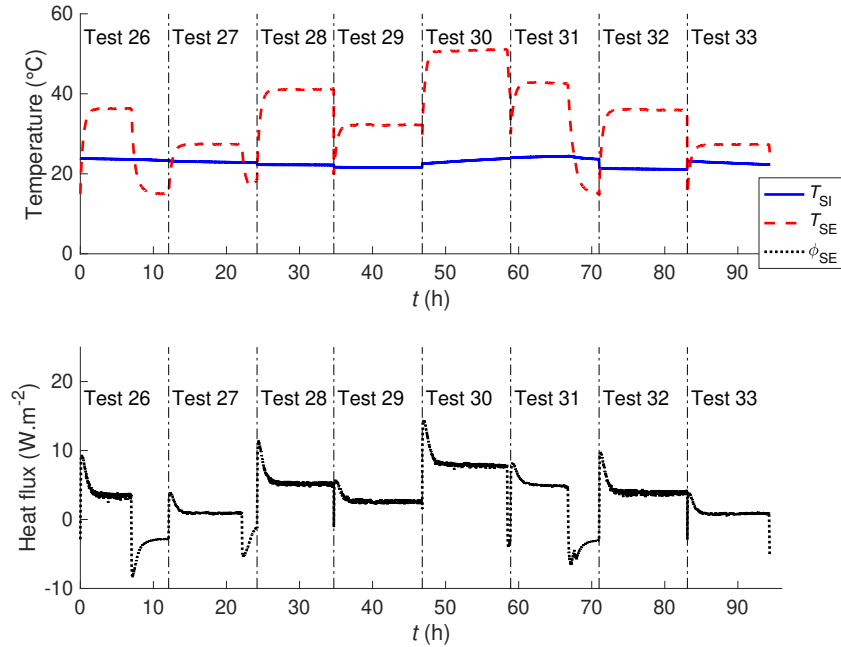


Figure 24: Measurement data of the **EIW** tests 26 to 33 under constant conditions.

its thermal resistance. Moreover, the poor estimation results obtained with the test 25 demonstrates that installing the measurement prototype on the external metal siding is not suitable to examine this wall due to the air gap. Then, for the tests 26 to 33 for which the metal siding is removed, the estimated resistance values are higher than the reference value and become closer to the theoretical resistance value calculated without metal frame (see Table 2). As discussed in Section 3.2, the reference value obtained by the GHB method takes into account the influence of the metal frames (with thermal bridge effects) so that it is logical that the measurements without metal frame return higher thermal resistance values.

4.3. WFW results under constant conditions

Fig. 26 shows the measurement data of the five tests on the WFW wall under three different constant conditions. The first two tests 44-45 are launched on a zone containing the thermal bridges (see Fig. 14), the absorbed heat flux values are higher than for the other three cases 46 to 48 tested on a

Table 12: Estimated thermal resistances and corresponding uncertainties by using 10-hour measurement data for the tests on the **EIW** under constant conditions (in $\text{m}^2\cdot\text{K}\cdot\text{W}^{-1}$, * obtained by linear regression) - ** IFSTTAR uncertainty value only allows to derive the lowest bound of the estimated thermal resistance.

Test	R_{theo}	R_{ref}	$R_{estim} (u_{Restim})$		
			CERTES	CSTB	IFSTTAR**
23	3.86	2.03*	0.59 (0.01)	0.82 (0.03)	4.68 (4.09)
24	3.86	2.03*	0.57 (0.01)	0.94 (0.04)	4.65 (4.12)
25	3.86	2.1	0.48 (0.06)	1.34 (0.08)	3.64 (1.89)
26	3.86	2.1	3.35 (0.03)	6.00 (1.45)	3.62 (0.66)
27	3.86	2.1	3.40 (0.01)	16.58 (0.36)	4.98 (2.37)
28	3.86	2.1	3.47 (0.09)	3.58 (0.03)	3.81 (0.97)
29	3.86	2.1	3.43 (0.08)	3.68 (0.03)	4.98 (2.38)
30	3.86	1.92*	3.16 (0.04)	2.69 (0.01)	3.78 (0.86)
31	3.86	1.92*	3.41 (0.02)	2.55 (0.01)	3.80 (1.09)
32	3.86	2.1	3.58 (0.08)	4.38 (0.18)	3.84 (0.88)
33	3.86	2.1	3.54 (0.03)	15.51 (0.01)	4.97 (2.36)

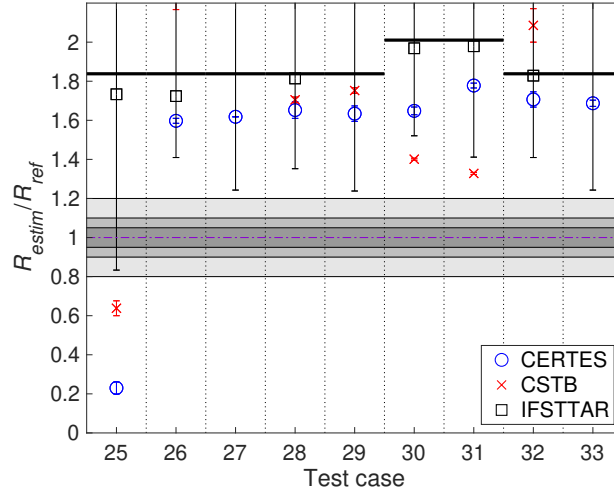


Figure 25: Estimated thermal resistances normalized by the reference value for the **EIW** tests under constant conditions by using 10-hour measurement data with an exterior solicitation (test 25 is performed on metal siding surface, tests 26 to 33 are performed on insulation surface, the bold horizontal black line refers to the ratio R_{theo}/R_{ref}).

homogeneous zone of the wall. Moreover, for the tests 44-45, internal surface temperature profiles show an increasing tendency, which is more important than the other three ones. These differences are caused by the presence of the thermal bridges which absorb more heat than the other parts of the wall.

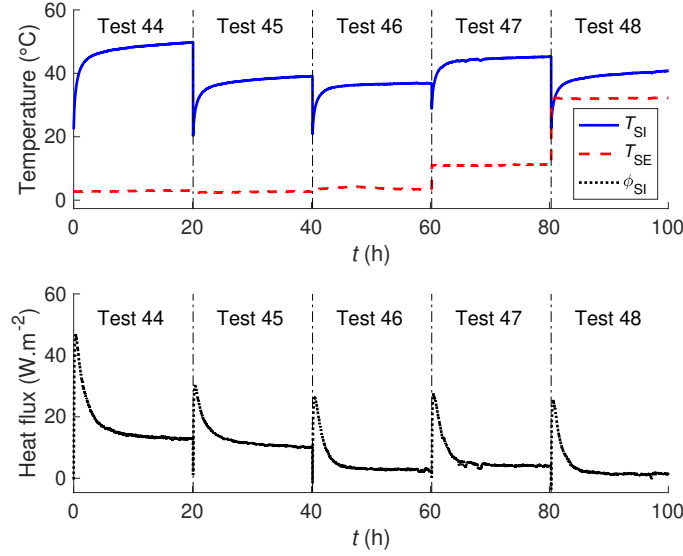


Figure 26: Measurement data of the WFW tests 44 to 48 under constant conditions.

Table 13 and Fig. 27 present the estimated thermal resistances and corresponding uncertainties for the five tests of this measurement series by using 10-hour measurement data. For all the identification methods the estimation results of tests 44-45 show clearly the effect of the thermal bridges. Only a small amount of the total thermal resistance is detected (between 20 and 65% depending on the method). The thermal bridge disturbs the longitudinal diffusion of the excitation heat flux and accelerates the lateral one because of its high thermal conductivity. These tests illustrate the remarkable influence of the thermal bridges on the thermal resistance estimation and the need to avoid them when measuring.

In the next tests 46 to 48, the active solicitation was conducted with 100% of heating power on a zone of the internal wall surface without thermal bridge. Concerning tests 46 and 47, it can be observed that the three identification methods give a thermal resistance value of about one half of the

Table 13: Estimated thermal resistances and corresponding uncertainties by using 10-hour measurement data for the tests on the WFW under constant conditions (in $\text{m}^2\cdot\text{K}\cdot\text{W}^{-1}$) - * IFSTTAR uncertainty value only allows to derive the lowest bound of the estimated thermal resistance.

Test	R_{theo}	R_{ref}	$R_{estim} (u_{R_{estim}})$		
			CERTES	CSTB	IFSTTAR*
44	9.11	7.6	1.70 (0.06)	2.44 (0.10)	4.93 (1.87)
45	9.11	7.6	1.50 (0.03)	2.61 (0.09)	4.07 (1.40)
46	9.11	7.6	3.18 (0.10)	4.26 (0.29)	5.19 (1.98)
47	9.11	7.1	3.94 (0.09)	4.84 (0.24)	5.56 (1.24)
48	9.11	6.7	3.55 (0.12)	1.82 (0.25)	5.29 (1.59)

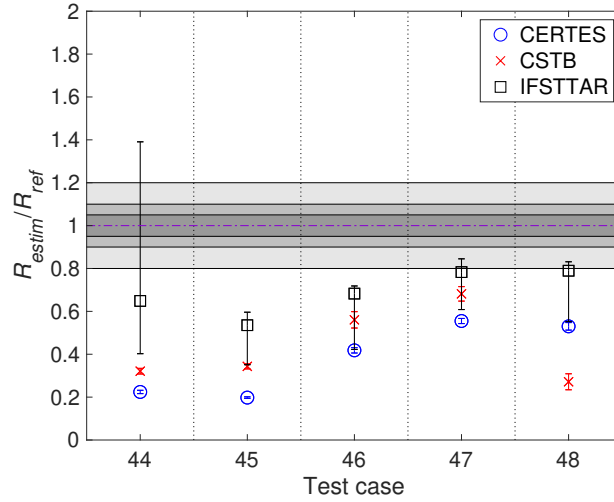


Figure 27: Estimated thermal resistances normalized by the reference value for the WFW tests under constant conditions by using 10-hour measurement data.

total thermal resistance of this wall. Hence, only the first insulation of the WFW can be determined using the proposed technique on a 10-hour time interval. To confirm this proposal, the measurement data of thermal sensors inside the WFW is analyzed. Fig. 28, which shows the temperature and heat flux measurements in the wall, indicates that there is no heat flux variation observed in the second insulation. The OSB layer between the two insulation layers diffuses mostly laterally the heat flux coming on its internal surface. Therefore, the first insulation layer is the only one that can be characterized

in the considered WFW. Lastly, for test 48 for which the outside temperature is higher than the indoor temperature, CSTB identification results are deteriorated whereas CERTES and IFSTTAR techniques have results similar to the ones of tests 46 and 47.

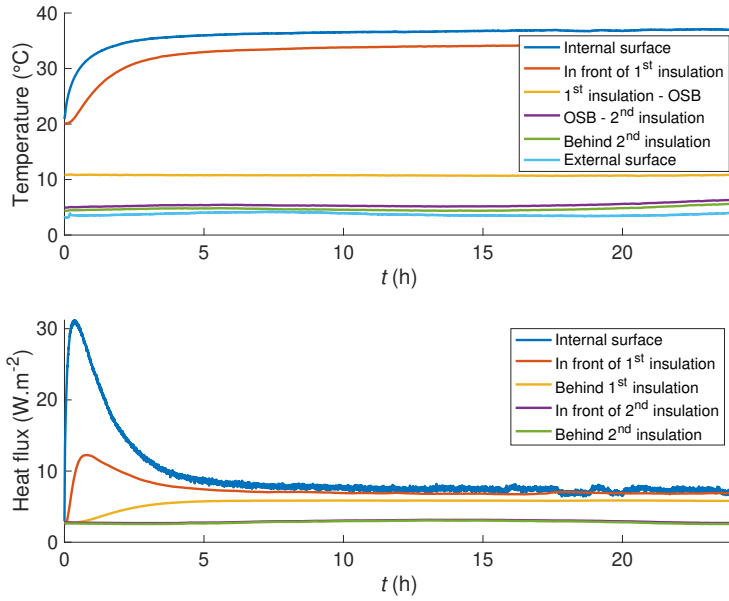


Figure 28: Measurement data of the thermal sensors inside the WFW.

4.4. *SCW* results

4.4.1. *Constant conditions*

Fig. 29 presents the measurement data of the four tests 34 to 37 on the *SCW* of a concrete building under constant conditions conducted in the Sense-City equipment. We can see slight fluctuations due to the ON/OFF regulation system of the building. Nevertheless, as the proposed measurement prototype uses the net absorbed heat flux and the indoor surface temperature, these fluctuations observed in Fig. 29 are taken into account in the identification process.

Table 14 and Fig. 30 present the estimation results of these tests and their corresponding uncertainties by using 6-hour measurement data. In the four

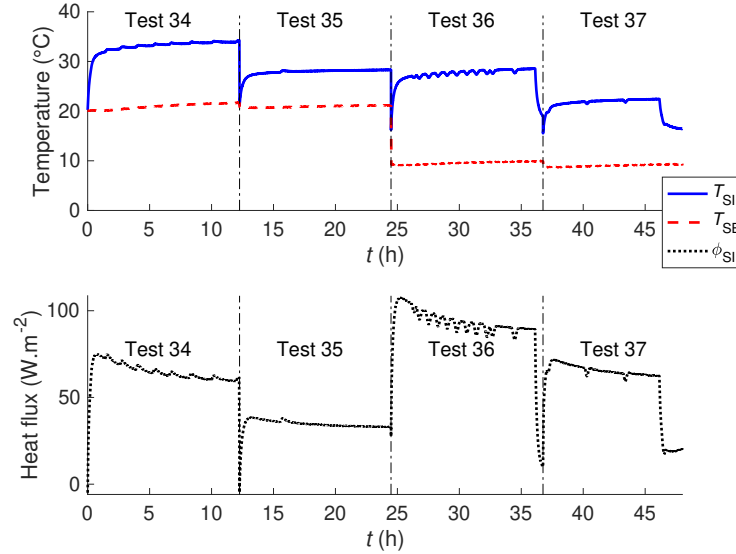


Figure 29: Measurement data of the **SCW** tests 34 to 37 under constant conditions.

tests, the estimated thermal resistance (resp. the lowest estimated thermal resistance) is accurately determined using CSTB and CERTES techniques (resp. IFSTTAR inverse technique), *i.e.* difference less than $0.1 \text{ m}^2 \cdot \text{K} \cdot \text{W}^{-1}$ compared to the reference value. Only the test 34 for CERTES method leads to a wrong estimation with an estimation result which is two times larger than the expected value. This test was performed under the same interior and exterior air temperatures (20°C) with the maximum heating power and produced the highest internal surface temperature. Thus, the air conditioner regulation was maximum during this test. Therefore, the measurement disturbance linked to the air conditioner was the most important in that case and the CERTES method seems to be the most sensitive to this disturbance.

4.4.2. Variable conditions

Fig. 31 shows the measurement data of the **SCW** tests under variable conditions using Sense-City climatic chamber. Temperature regulation inside the building only ensures a quasi constant internal air temperature. However, as presented in Section 3.1.2, the climatic chamber Sense-City allows controlling the external air temperature and adding artificial solar radiation

Table 14: Estimated thermal resistances and corresponding uncertainties by using 6-hour measurement data for the tests on the **SCW** under constant conditions (in $\text{m}^2\cdot\text{K}\cdot\text{W}^{-1}$) - * IFSTTAR uncertainty value only allows to derive the lowest bound of the estimated thermal resistance.

Test	R_{theo}	R_{ref}	$R_{estim} (u_{R_{estim}})$		
			CERTES	CSTB	IFSTTAR*
34	0.14	0.25	0.49 (0.06)	0.18 (0.01)	0.88 (0.71)
35	0.14	0.25	0.21 (0.02)	0.18 (0.01)	0.73 (0.54)
36	0.14	0.25	0.20 (0.01)	0.20 (0.01)	0.73 (0.51)
37	0.14	0.25	0.21 (0.01)	0.21 (0.01)	0.71 (0.49)

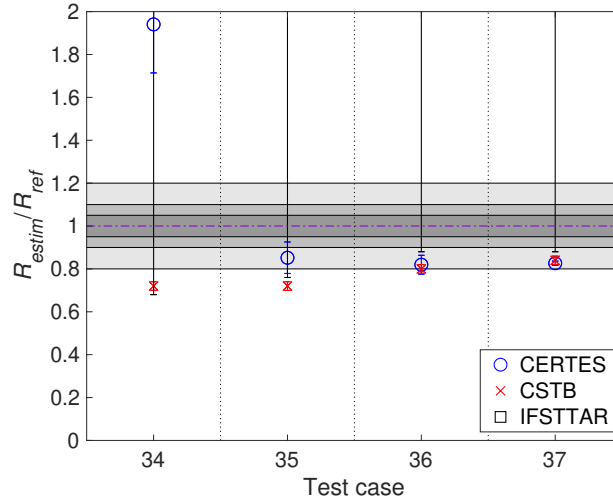


Figure 30: Estimated thermal resistance normalized by the reference value for the **SCW** tests under constant conditions by using 6-hour measurement data.

on the wall external surface. Let us note that the same external temperature T-Var. 6 presented in Fig. 11 is considered in the tests 38 to 41. The last two ones 40-41 involve a small amount of solar radiation provided by a powerful lamp system at the ceiling of the climatic chamber. Therefore, for these last two tests, the increase of external surface temperature is greater than for the first two ones. Moreover, it can be observed that the fluctuations due to temperature regulation inside the building under variable conditions are more important here than under constant conditions.

According to the estimation results presented in Table 15 and Fig. 32,

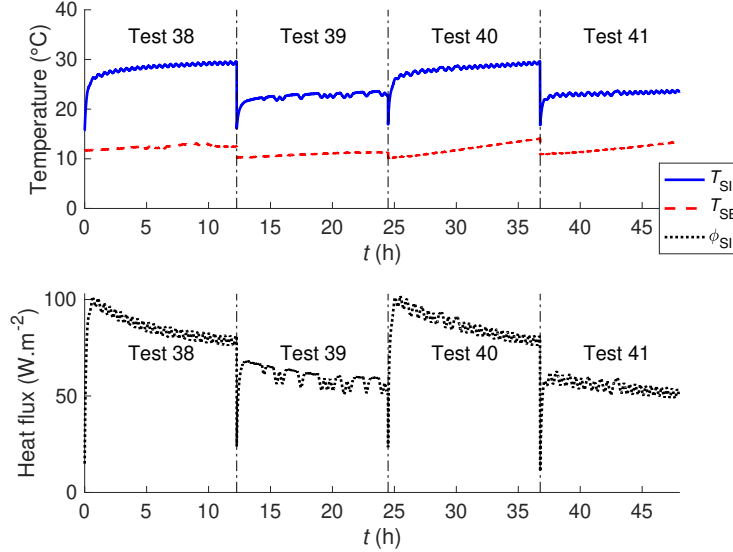


Figure 31: Measurement data of the **SCW** tests 38 to 41 under variable conditions.

the prototype proposed in this paper and the three identification techniques are generally able to provide an acceptable thermal resistance value (gap between reference and estimated value less than $0.5 \text{ m}^2 \cdot \text{K} \cdot \text{W}^{-1}$) after 6 hours of measurement. The heating power does not seem to have a significant impact on the estimation. Nevertheless, the CERTES estimation result for test 39 is too large compared to the expected value. As observed in Fig. 31, the signal to noise ratio of the measurements in this test is the lowest of the four tests, which could explain this incorrect estimation result. Consequently, the uncertainty values are higher for this test for the CERTES method. Moreover in presence of solar radiation in tests 40 and 41, IFSTTAR technique gives less accurate results.

4.4.3. Natural conditions

After running measurement in the climatic chamber, the **SCW** of Sense-City concrete building is tested under natural conditions by removing the climatic chamber. The indoor building temperature is maintained at 20°C and no solar protection is used in these cases. The measurement data of these **SCW** tests are presented in Fig. 33. These data sets are quite similar

Table 15: Estimated thermal resistances and corresponding uncertainties by using 6-hour measurement data for the tests on the **SCW** under variable conditions (in $\text{m}^2.\text{K}.\text{W}^{-1}$) - * IFSTTAR uncertainty value only allows to derive the lowest bound of the estimated thermal resistance.

Wall	Test	R_{theo}	R_{ref}	$R_{estim} (u_{Restim})$		
				CERTES	CSTB	IFSTTAR*
SCW	38	0.14	0.25	0.18 (0.01)	0.20 (0.01)	0.74 (0.58)
	39	0.14	0.25	0.34 (0.04)	0.19 (0.01)	0.72 (0.52)
	40	0.14	0.25	0.25 (0.01)	0.20 (0.01)	0.75 (0.38)
	41	0.14	0.25	0.24 (0.01)	0.22 (0.02)	0.71 (0.34)

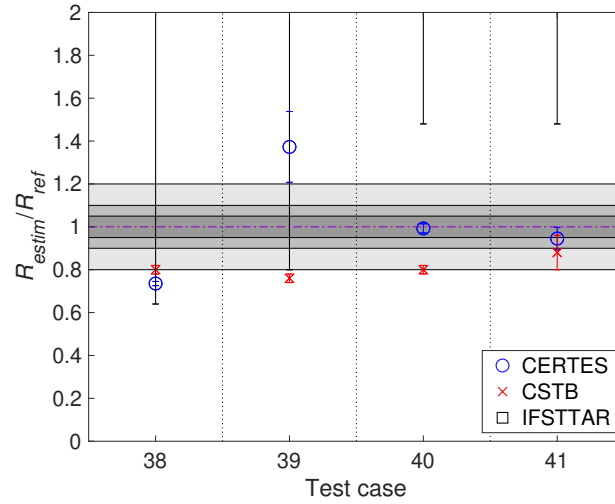


Figure 32: Estimated thermal resistance normalized by the reference value for the **SCW** tests under variable conditions by using 6-hour measurement data.

to the previous tests performed on this wall.

Table 16 shows the estimated thermal resistances obtained for these tests. Although all the values obtained are beyond 20% error compared to the reference value, the estimation of **SCW** thermal resistance in natural conditions can be considered as “appropriate”. Indeed, recalling that the reference value is $0.25 \text{ m}^2.\text{K}.\text{W}^{-1}$, we note that the three identification methods successfully detected the **SCW** thermal resistance to be less than $0.75 \text{ m}^2.\text{K}.\text{W}^{-1}$ (except for CERTES technique in test 42). The **SCW** wall contains only a concrete layer whose thermal inertia is quite weak. Thus, significant solar radiation

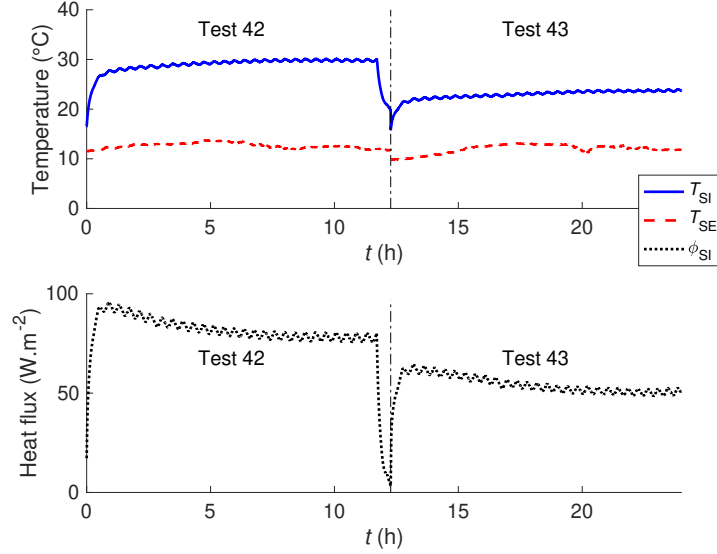


Figure 33: Measurement data of the **SCW** tests 42 to 43 under natural conditions.

has a rapid impact through the wall thickness. So, it appears that solar protection is recommended for this type of wall under natural environmental conditions.

Table 16: Estimated thermal resistances and corresponding uncertainties by using 6-hour measurement data for the tests on the **SCW** under natural conditions (in $\text{m}^2 \cdot \text{K} \cdot \text{W}^{-1}$) - * IFSTTAR uncertainty value only allows to derive the lowest bound of the estimated thermal resistance.

Wall	Test	R_{theo}	R_{ref}	$R_{estim} (u_{R_{estim}})$		
				CERTES	CSTB	IFSTTAR*
SCW	42	0.14	0.25	8.56 (3.34)	0.19 (0.01)	0.74 (0.41)
	43	0.14	0.25	0.56 (0.01)	0.17 (0.01)	0.65 (0.37)

In conclusion, it can be underlined that the proposed measurement prototype was able to identify the poorly insulated nature of the studied **SCW** under different environmental conditions.

5. Conclusions and perspectives

In a previous article [36], a strategy was proposed for *in situ* identification of the thermal resistance of building wall and first virtual tests were performed using a numerical benchmark. From the results obtained, a real measurement prototype was developed. In the proposed identification protocol, an active solicitation using lights is applied to the inside face of the wall while the inside surface temperature and the net absorbed heat flux are recorded. The thermal characteristics of the wall are determined by three different inverse techniques (CERTES, CSTB, IFSTTAR) combining sensor outputs and simple physical models. Thanks to an aluminum plate placed in contact with the inside wall face, the imposed thermal excitation can be homogenized before being transmitted to the wall surface. Moreover, it allows to get more robust identification results as: (i) it is less sensitive to the internal exchange coefficient; (ii) it can reduce significantly the measurement noise and (iii) it limits the effects of the environment. The objective of this article was to deeply evaluate the abilities and the limits of this measurement device to determine, in a reduced time period, the thermal resistance of different wall typologies in several conditions. First experiments conducted on a real doubling wall in laboratory showed that the wall thermal resistance can be properly determined in less than 10 h.

Different real conventional walls, *i.e.* **IIW**, **EIW**, **WFW** and **SCW**, were tested under constant, variable and natural conditions. The identified thermal resistance were compared to reference values notably determined from Guarded Hot Box equipment. Concerning the active solicitation, two different heating levels were studied. In general, it showed that the heating power has not a significant influence on the estimation precision. Nevertheless, due to the short time of excitation and important lateral heat flux in the wall which are not taken into account in the considered physical models, we observed that only the first layers of the wall can be characterized in the proposed identification process. Hence, the measurement prototype gives the more accurate thermal resistance estimation for the **IIW** as the insulation is positioned on the inside **and as it is made of homogeneous layers without any thermal bridge**. For the **EIW**, acceptable estimation of the thermal resistance can be obtained by adapting the experimental protocol. The prototype, *i.e.* active solicitation and measurement, should be installed on the exterior surface in order to determine accurately the thermal characteristics of the exterior insulation. Concerning the high-insulated **WFW**, the

results indicate that there is no variation of heat flux in the second insulation layer. The OSB layer located between the two insulation layers diffuses mostly the heat flux from its internal surface. Therefore, the first layer is the only one that can be characterized with this configuration of WFW wall by means of the proposed experimental set-up. Lastly, the proposed techniques were able to identify the poorly insulated nature of the Sense-City concrete building SCW in constant, variable and natural environmental conditions. To sum up, with regards to the numerical inverse techniques, we noted that identification results can be less precise using IFSTTAR method compared to CERTES and CSTB approaches but IFSTTAR method gives a robust estimation of the minimum value of the wall thermal resistance.

For operational purposes, thermal bridges should be avoided in the measurement zone because it may lower the estimated thermal resistance because of high thermal absorption. In addition, this prototype shows the possibility of testing under variable and natural conditions. However, in order to obtain an improved estimation, a solar protection of $60 \times 60 \text{ cm}^2$ on the outside of the wall (instead of completely covering the external surface) is necessary to reduce the disturbances from solar radiation. Another solution can be to choose the nighttime to launch the measurement.

In perspective, the size of the prototype must to be reduced by using surface heating resistance instead of lights. *In situ* tests will be conducted on real occupied buildings. Measurement, physical and numerical developments are to be carried out in order to characterize high-insulated walls, *i.e.* thermal resistance higher than $6 \text{ m}^2 \cdot \text{K} \cdot \text{W}^{-1}$, and other wall categories like bio-sourced and raw earth walls.

Acknowledgments

These works realized in the project named “RESBATI” were funded by the French National Research Agency (ANR). The authors also acknowledge the support from the project “Sense-City” funded by ANR (France) within the Investment for the Future Program under reference number ANR-10-EQPX-48.

References

- [1] *European Commission - Eurostat [Online]*. Available: <https://ec.europa.eu/eurostat/web/main/home>.

- [2] *Réglementation Thermique RT 2012*. Ed. Centre Scientifique et Technique du Bâtiment, 2012 (in French).
- [3] *PERFORMER Project*. “Portable, Exhaustive, Reliable Flexible and Optimized approach to Monitoring and Evaluation of building energy performance”, 2014.
- [4] S. Roels. *The IEA EBC Annex 58 - project on “Reliable building energy performance characterisation based on full scale dynamic measurements”*. IEA Annex 58 Seminar - Real building energy performance assessment, Gent, 2014.
- [5] J. Berger, S. Tasca-Guernouti, M. Humbert. *Experimental method to determine the energy envelope performance of building*. 10th International Conference for Enhanced Building Operations, Kuwait, 2010.
- [6] P. Bacher, H. Madsen. *Identifying suitable models for the heat dynamics of buildings*. Energy and Buildings, vol. 43(7), pp. 1511-1522, 2011.
- [7] S. Thébault, R. Bouchié. *Refinement of the ISABELE method regarding uncertainty quantification and thermal dynamics modelling*. Energy and Buildings, vol. 178, pp. 182-205, 2018.
- [8] F. Alzetto, J. Meulemans, G. Pandraud, D. Roux. *A perturbation method to estimate building thermal performance*. C. R. Chimie, vol. 21, pp. 938-942, 2018.
- [9] C. K. Basak, G. Sarkar, S. Neogi. *Performance evaluation of material and comparison of different temperature control strategies of a Guarded Hot Box U-value Test Facility*. Energy and Buildings, vol. 105, pp. 258-262, 2015.
- [10] I. Naveros, M. J. Jiménez, M. R. Heras. *Analysis of capabilities and limitations of the regression method based in averages, applied to the estimation of the U value of building component tested in Mediterranean weather*. Energy and Buildings, vol. 55, pp. 854-872, 2012.
- [11] P. G. Cesaratto, M. De Carli. *A measuring campaign of thermal conductance in situ and possible impacts on net energy demand in buildings*. Energy and Buildings, vol. 59, pp 29-36, 2013.

- [12] D. Bienvenido-Huertas, J. Moyano, C. E. Rodriguez-Jimenez, D. Marin. *Applying an artificial neural network to assess thermal transmittance in walls by means of the thermometric method*. Applied Energy, vol. 233-234, pp. 1-14, 2019.
- [13] *ISO 8990:1994*. Thermal insulation - Determination of steady-state thermal transmission properties - Calibrated and guarded hot box, ISO standard, 1994.
- [14] *ISO 9869-1:2014*. Thermal insulation - Building elements - In-situ measurement of thermal resistance and thermal transmittance - Part 1: Heat flow meter method, ISO standard, 2014.
- [15] *ISO 9869-2:2018*. Thermal insulation - Building elements - In-situ measurement of thermal resistance and thermal transmittance - Part 2: Infrared method for frame structure dwelling, ISO standard, 2018.
- [16] I. Danielski, M. Froling. *Diagnosis of buildings thermal performance - A quantitative method using thermography under non-steady state heat flow*. Energy Procedia, vol. 83, pp. 320-329, 2015.
- [17] R. Albatici, A. M. Tonelli, M. Chiogna. *A comprehensive experimental approach for the validation of quantitative infrared thermography in the evaluation of building thermal transmittance*. Applied Energy, vol. 141, pp. 218-228, 2015.
- [18] I. Nardi, S. Sfarra, D. Ambrosini. *Quantitative thermography for the estimation of the u-value: State of the art and a case study*. Journal of Physics Conference, vol. 547, pp. 1-8, 2014.
- [19] A. Nowoswiat, J. Skrzypczyk, P. Krause, T. Steidl, A. Winkler-Skalna. *Estimation of thermal transmittance based on temperature measurements with the application of perturbation numbers*. Heat and Mass Transfer, vol. 54, pp. 1477-1489, 2017.
- [20] P. A. Fokaides, S. A. Kalogirou. *Application of infrared thermography for the determination of the overall heat transfer coefficient (U-value) in building envelopes*. Applied Energy, vol. 88, pp. 4358-4365, 2011.
- [21] B. Tejedor, M. Casals, M. Macarulla, A. Giretti. *U-value time series analyses: Evaluating the feasibility of in-situ short-lasting IRT tests*

- for heavy multi-leaf walls. *Building and Environment*, vol. 159, 106123, 2019.
- [22] *ISO 6946:2017*. Building components and building elements - Thermal resistance and thermal transmittance - Calculation methods, ISO standard, 2017.
- [23] Z. Petojevic, R. Gospavic, G. Todorovic. *Estimation of thermal impulse response of a multi-layer building wall through in-situ experimental measurements in a dynamic regime with applications*. *Applied Energy*, vol. 228, pp. 468-486, 2018.
- [24] M. H. A. Larbi Youcef, V. Feuillet, L. Ibos, Y. Candau. *In situ quantitative diagnosis of insulated building walls using passive infrared thermography*. *Quantitative InfraRed Thermography Journal*, DOI: 10.1080/17686733.2020.1805939, 2020.
- [25] P. Biddulph, V. Gori, C. A. Elwell, C. Scott, C. Rye, R. Lowe, T. Oreszczyn. *Inferring the thermal resistance and effective thermal mass of a wall using frequent temperature and heat flux measurements*. *Energy and Buildings*, vol. 78, pp. 10-16, 2014.
- [26] V. Gori, C. A. Elwell. *Estimation of thermophysical properties from in-situ measurements in all seasons: Quantifying and reducing errors using dynamic grey-box methods*. *Energy and Buildings*, vol. 167, pp. 290-300, 2018.
- [27] L. De Simon, M. Iglesias, B. Jones, C. Wood. *Quantifying uncertainty in thermophysical properties of walls by means of Bayesian inversion*. *Energy and Buildings*, vol. 177, pp. 220-245, 2018.
- [28] E. Sassine. *A practical method for in-situ thermal characterization of walls*. *Case Studies in Thermal Engineering*, vol. 8, pp. 84-93, 2016.
- [29] K. Chaffar, A. Chauchois, D. Defer, L. Zalewski. *Thermal characterization of homogeneous walls using inverse method*. *Energy and Buildings*, vol. 78, pp. 248-255, 2014.
- [30] M. H. A. Larbi Youcef, V. Feuillet, L. Ibos, Y. Candau, P. Balcon, A. Filloux. *Quantitative diagnosis of insulated building walls of restored old*

constructions using active infrared thermography. Quantitative InfraRed Thermography Journal, vol. 8(1), pp. 65-87, 2011.

- [31] A. Rasooli, L. Itard, C. I. Ferreira. *A response factor-based method for the rapid in-situ determination of wall's thermal resistance in existing buildings*. Energy and Buildings, vol. 119, pp. 51-61, 2016.
- [32] A. Rasooli, L. Itard. *In-situ rapid determination of walls' thermal conductivity, volumetric heat capacity, and thermal resistance, using response factors*. Applied Energy, vol. 253, 2019.
- [33] J. Meulemans, F. Alzetto, D. Farmer, C. Gorse. *QUB/e - A novel transient experimental method for in situ measurements of the thermal performance of building fabrics* in: C. Gorse, M. Dastbaz (Eds.), Building Information Modelling, Building Performance, Design and Smart Construction, Springer, Cham, Switzerland, 2017.
- [34] A. François, L. Ibos, V. Feuillet, J. Meulemans. *Estimation of the thermal resistance of a building wall with inverse techniques based on rapid in situ measurements and white-box or ARX black-box models*. Energy and Buildings, vol. 226, 110346, 2020.
- [35] E. Biteau, D. Defer, F. Brachelet, L. Zalewski, *Active Thermal Method Applied to the In Situ Characterization of Insulating Materials in a Wall*. Buildings, vol. 11, 578, 2021.
- [36] T.-T. Ha, V. Feuillet, J. Waeytens, K. Zibouche, S. Thébault, R. Bouchié, V. Le Sant, L. Ibos. *Benchmark of identification methods for the estimation of building wall thermal resistance using active method: numerical study for IWI and single-wall structures*. Energy and Buildings, vol. 224, 110130, 2020.
- [37] T.-T. Ha, L. Ibos, V. Feuillet, Y. Garcia, V. Le Sant, A. Koenen, L. Peiffer, R. Bouchié, K. Zibouche, J. Waeytens. *Experimental works with new prototype for measuring thermal resistance of building walls*. Congrès de la Société Française de Thermique, 2020.
- [38] Z. Djatouti, J. Waeytens, L. Chamoin, P. Chatellier. *Goal-oriented sensor placement and model updating strategies applied to a real building in the Sense-City equipment under controlled winter and heat wave scenarios*. Energy and Buildings, vol. 231, 110486, 2021.

- [39] S. Martinez, A. Erkoreka, P. Eguia, E. Granada, L. Febrero. *Energy characterization of a PASLINK test cell with a gravel covered roof using a novel methodology: Sensitivity analysis and Bayesian calibration*. Journal of Building Engineering, vol. 22, pp. 1-11, 2019.
- [40] W. Li, Z. Tian, Y. Lu, F. Fu. *Stepwise calibration for residential building thermal performance model using hourly heat consumption data*. Energy and Buildings, vol. 181, pp. 10-25, 2018.
- [41] M. Kristensen, S. Petersen. *Choosing the appropriate sensitivity analysis method for building energy model-based investigations*. Energy and Buildings, vol. 176, pp. 130-166, 2016.
- [42] J. Brouns, A. Nassiopoulos, F. Bourquin, K. Limam, *Dynamic building performance assessment using calibrated simulation*. Energy and Buildings, vol. 122, pp. 160-174, 2016.
- [43] A. Nassiopoulos, R. Kuate, F. Bourquin, *Calibration of building thermal models using an optimal control approach*. Energy and Buildings, vol. 76, pp. 81-91, 2014.
- [44] A. N. Tikhonov, Y. Arsenin. *Solution to ill-posed problems*, Ed. Winston-Widley, 1977.
- [45] S. Demeyer, V. Le Sant, A. Koenen, N. Fischer, J. Waeytens, R. Bouchié. *Bayesian uncertainty analysis of inversion models applied to the inference of thermal properties of walls*. Energy and Buildings, vol. 249, 111188, 2021.
- [46] J. Berger, H. R. B. Orlande, N. Mendes, S. Guernouti. *Bayesian inference for estimating thermal properties of a historic building wall*. Building and Environment, vol. 106, pp. 327-339, 2016.
- [47] M. Vihola. *Robust adaptive metropolis algorithm with coerced acceptance rate*. Statistics and Computing, vol. 22, pp. 997-1008, 2012.
- [48] *CTSM-R: Continuous-Time Stochastic Modelling for R*. stsm.info.
- [49] *ISO 8302:1991*. Thermal insulation — Determination of steady-state thermal resistance and related properties — Guarded hot plate apparatus, ISO standard, 1991.

- [50] S. E. Gustafsson. *Transient plane source techniques for thermal conductivity and thermal diffusivity measurements of solid materials*. Review of Scientific Instruments, vol. 62(3), pp. 797-804, 1991.
- [51] P. De Wilde. *The gap between predicted and measured energy performance of buildings: A framework for investigation*. Automation in Construction, vol. 41, pp. 40-49, 2014.
- [52] D. Johnston, D. Miles-Shenton, D. Farmer. *Quantifying the domestic building fabric 'performance gap'*. Building Services Engineering Research and Technology, vol. 36(5), pp. 614-627, 2015.
- [53] *Boîte chaude gardée. Nouvel équipement au service de la transition énergétique*. <https://www.cstb.fr/assets/documents/cstb-boite-chaude-gardee.pdf>, 2020 (in French).